Int J Thermophys (2009) 30:737–781
DOI 10.1007/s10765-009-0602-6

Experimental Study of the Critical Behavior of the Isochoric Heat Capacity of Aqueous Ammonia Mixture

N. G. Polikhronidi · I. M. Abdulagatov · R. G. Batyrova · G. V. Stepanov

Received: 25 March 2009 / Accepted: 15 May 2009 / Published online: 4 June 2009

Abstract The isochoric heat capacity of a $NH_3 + H_2O$ (0.2607 mole fraction of ammonia) mixture has been measured in the near- and supercritical regions. Measurements were made in the single- and two-phase regions including the coexistence curve using a high-temperature, high-pressure, nearly constant-volume adiabatic calorimeter. Measurements were made along 38 liquid and vapor isochores in the range from 120.03 kg · m^{-3} to 671.23 kg · m^{-3} and at temperatures from 478 K to 634 K and at pressures up to 28 MPa. Temperatures at the liquid–gas phase transition curve, $T_S(\rho)$, for each measured density (isochore) and the critical parameters (T_C and ρ_C) for the $0.2607\,NH_3 + 0.7393\,H_2O$ mixture were obtained using the quasi-static thermograms technique. The expanded uncertainty of the heat-capacity measurements at the 95 % confidence level with a coverage factor of $k = 2$ is estimated to be 2 % to 3 % in the near-critical and supercritical regions, 1.0 % to 1.5 % in the liquid phase, and 3 % to 4 % in the vapor phase. Uncertainties of the density, temperature, and concentration measurements are estimated to be 0.06 %, 15 mK, and 5×10^{-5} mole fraction, respectively. An unusual behavior of the isochoric heat capacity of the mixture was found near the maxcondetherm point (in the retrograde region). The value of the Krichevskii parameter was calculated using the critical properties data for the mixture and vapor-pressure

N. G. Polikhronidi · I. M. Abdulagatov · R. G. Batyrova · G. V. Stepanov
Institute of Physics of the Dagestan Scientific Center of the Russian Academy of Sciences, Makhachkala, Dagestan, Russia

I. M. Abdulagatov
Geothermal Research Institute of the Dagestan Scientific Center of the Russian Academy of Sciences, Makhachkala, Dagestan, Russia

Present Address:
I. M. Abdulagatov (✉)
Thermophysical Properties Division, National Institute of Standards and Technology, 325 Broadway, Boulder, CO 80305, USA
e-mail: ilmutdin@boulder.nist.gov

data for the pure solvent (H_2O). The derived value of the Krichevskii parameter was used to analyze the critical behavior of the strong (C_P, K_T) and weakly (C_V) singular properties in terms of the principle of isomorphism of critical phenomena in binary mixtures. The values of the characteristic parameters (K_1, K_2), temperatures (τ_1, τ_2), and the characteristic density differences ($\Delta\rho_1$, $\Delta\rho_2$) were calculated for the $NH_3 + H_2O$ mixture by using the critical-curve data.

Keywords Ammonia · Binary mixture · Coexistence curve · Critical parameters · Critical point · Equation of state · Isochoric heat capacity · Krichevskii parameter · Maxcondetherm · Quasi-static thermograms · Retrograde phenomena · Water

1 Introduction

Power cycles with $NH_3 + H_2O$ mixtures as working fluids have been shown to reach higher thermal efficiencies than the traditional steam turbine (Rankine) cycle with water as the working fluid [1–14]. The efficiency of the Kalina cycle is from 1.6 to 1.9 times higher than that of the Rankine cycle system, at the same boundary conditions. The best $NH_3 + H_2O$ cycle produced approximately 40 % to 70 % more power than a single-pressure steam cycle and 20 % to 25 % more power than a dual-pressure steam cycle. Different thermodynamic properties data (correlations and equation of state) reported by various authors have been used in studies of $NH_3 + H_2O$ mixture cycles. The differences in thermal efficiencies for a bottoming Kalina cycle when various thermodynamic properties are used are in the range from 0.5 % to 3.5 %.

In design and analysis of geothermal cycles (Kalina power cycle), accurate thermodynamic properties are required for $NH_3 + H_2O$ mixtures at temperatures from 283 K to 866 K and at pressures up to 22 MPa. The thermodynamic properties of ammonia and water mixtures are suitable for a power cycle working fluid mixture. For example, the substances are soluble in each other and easily separable. Ammonia and water have different boiling temperatures; thus, the $NH_3 + H_2O$ mixture evaporates over a large temperature range, which is an advantage for power generation from a sensible heat source. Ammonia and water form a non-azeotropic mixture.

In order to calculate the thermodynamic performance of an $NH_3 + H_2O$ cycle, an accurate equation of state (EOS) for the working fluid is required. All the available EOS give similar results at low temperatures and low pressures, while the differences increase at high temperatures and high pressures (near the critical points). An accurate determination of the locations of the dew and bubble curves is extremely important to know, so that no liquid forms when the fluid expands in the turbine. The study also found that the optimum fluids for a resource tend to be those that have a supercritical cycle. For this reason, it is necessary to accurately construct a thermodynamic surface for the $NH_3 + H_2O$ mixture at all compositions near the critical points and at supercritical conditions. In this study we studied the isochoric heat capacity of an $NH_3 + H_2O$ mixture near the critical point, which is very important to accurately develop a crossover EOS. Water and ammonia are strongly polar fluids. The gas-phase dipole moment at the normal boiling point (NBP) is 1.855 D for water and 1.470 D for ammonia. The acentric factor is 0.3443 for water and 0.2561 for ammonia.

IAPWS Certified Research Need (ICRN) #6 (September 2000) stated that data for $NH_3 + H_2O$ mixtures are very limited in the important supercritical region. Also, as concluded by Tillner-Roth and Friend [15], the available experimental data are not sufficient to establish an accurate equation of state. In addition to density measurements, measurements of caloric properties are also required. Most datasets show large scatter or systematic deviations from each other. The largest gap in the database is found in the single-phase regions. Measurements in the vapor and especially, in the supercritical, regions are needed to establish a reliable EOS for $NH_3 + H_2O$ mixtures. Thus, the main objective of the article is to provide new accurate experimental isochoric heat capacity ($C_V VT$) data, phase boundary (T_S, ρ_S) properties, and critical (T_C, ρ_C) parameters for a 0.2607 NH_3 + 0.7393 H_2O mixture using a high-temperature, high-pressure, nearly constant-volume adiabatic calorimeter that allows precise measurements near the liquid–gas critical point [16–26].

1.1 Review of Available Experimental Data

Although a significant amount of work has now been completed on the $NH_3 + H_2O$ system, including the IAPWS document describing a full thermodynamic surface for the mixture, additional work on this system would be very useful to develop an accurate reference EOS. There are still essentially no results for $C_V VT$ measurements in the supercritical region for this system. Isochoric heat-capacity ($C_V VT$) and phase boundary (T_S, ρ_S) data of $NH_3 + H_2O$ near the critical point are extremely scarce. A literature survey revealed that there is only one dataset for the isochoric heat capacity ($C_V VT$) of $NH_3 + H_2O$ mixtures, which is reported by Magee and Kagawa [27]. Measurements were made for three compositions of (0.7, 0.8, and 0.9) mole fraction of ammonia at temperatures between 300 K and 520 K by means of a vacuum adiabatic calorimeter. The expanded relative uncertainty (with a coverage factor of $k = 2$) and thus a two-standard-deviation estimate for the isochoric heat capacity is estimated to be 1 % for the liquid phase and 4 % for gaseous results.

A comprehensive thermodynamic data compilation for $NH_3 + H_2O$ mixtures has been reported by Tillner-Roth and Friend [15]. All the available thermodynamic data sources published before 1995 were critically analyzed and compared with each other. Most datasets show large scatter or systematic deviations from each other. The largest gap in the database is for caloric property measurements in the single-phase regions, especially in the vapor and supercritical regions. No isochoric heat-capacity data were published before 1998. All previous EOS for $NH_3 + H_2O$ mixtures were developed without accurate $C_V VT$ data; therefore, these EOS cannot be used to accurately calculate the caloric properties of $NH_3 + H_2O$ mixtures, especially in the critical and supercritical regions where a scaling-type critical anomaly of thermodynamic properties is observed. Also, all previous EOS were not examined for accuracy of the isochoric heat-capacity representation. Therefore, here we will briefly review only work where the isochoric heat-capacity, phase-boundary, and critical-properties data were reported after 1998. Below, we also briefly review the available EOS for this system.

1.2 Equations of State

The following types of EOS have been applied to represent the thermodynamic properties of mixtures: multiparametric fundamental EOS [28], crossover models [29,30], classical cubic EOS [31–33], virial-type EOS [34], perturbation theory EOS [35], group contribution EOS [36], law of corresponding states [37,38], and polynomial-type EOS [39]. A fundamental multiparametric equation of state (IAPWS recommended) for the Helmholtz free energy $A(V, T)$ of $NH_3 + H_2O$ mixtures, as reported by Tillner-Roth and Friend [28], represents the thermodynamic properties of the mixture in the temperature range from the solid–liquid–vapor boundary to the critical locus at pressures up to 40 MPa. The uncertainty of the calculated values of density is 0.3 %. The uncertainty of liquid and vapor mole fractions is about 0.01. This formulation provides the most accurate representation of the thermodynamic properties of the $NH_3 + H_2O$ system over a wide range of concentration, pressure, and temperature. Kiselev and Rainwater [29] applied the parametric crossover model for the $NH_3 + H_2O$ system. Due to the lack of reliable data in the critical region, Kiselev and Rainwater [29] used an isomorphic generalization of the extended law of corresponding states. The model's parameters were determined using the critical curve data. Therefore, the model cannot accurately represent the isochoric heat-capacity data near the critical point. Rainwater and Tillner-Roth [30] developed a correlation of this mixture property by combining the Leung–Griffiths model and a multiparametric Helmholtz free energy equation of state. As the authors stated, due to lack of experimental heat-capacity data in the critical region, it is impossible to develop an accurate crossover model for this mixture.

Enick et al. [40] developed a Peng–Robinson-type EOS for the $NH_3 + H_2O$ system to accurately predict the phase equilibrium properties. Thomsen and Rasmussen [41] developed an extended UNIQUAC model (electrolyte model) which combined the original UNIQUAC model, the Debye–Huckel law, and the Soave–Redlich–Kwong EOS. The model was limited to temperatures below the critical temperature of ammonia. The model was developed with consideration of the speciation equilibria (hydrolysis of ammonia). This model can be used to describe the excess enthalpy and heat capacity very accurately. Suzuki and Uematsu [42] proposed an EOS for $NH_3 + H_2O$ mixtures which is expressed by the Helmholtz free energy as a function of T, V, and x. The uncertainty in $PVTx$ properties is $0.02\,\rho$. Barhoumi et al. [43] used the Gibbs free energy function to model the thermodynamic properties of the $NH_3 + H_2O$ mixture. The model describes with good accuracy the mixture properties in the liquid and vapor phases and for liquid–vapor saturation at temperatures from 200 K to 500 K and at pressures up to 10 MPa. For the liquid phase, a three-parametric Margules model for the excess free enthalpy was formulated, while for the vapor phase, the virial EOS in pressure, truncated after the third term, was used.

Xu and Goswami [44] proposed a new method for thermodynamic property calculations of the water–ammonia mixture using the Gibbs free energy and empirical equations for bubble- and dew-point temperatures. Recently, Mejbri and Bellagi [45] reported modeling of the thermodynamic properties of the water–ammonia mixture by three different approaches: (a) empirical Gibbs free enthalpy model; (b) a semi-empirical Patel and Teja cubic EOS; and (c) a theoretical approach formulated as perturbed

chain statistical associating fluid theory (PC-SAFT) EOS. The PC-SAFT EOS demonstrates excellent capability to extrapolate to very high temperatures and pressures (Kalina cycle conditions), while the Gibbs free enthalpy model was recommended for use for industrial applications such as absorption refrigeration.

1.3 Critical Parameters

Previously, the critical properties of $NH_3 + H_2O$ solutions were measured by several authors [46–51]. Most critical parameters of the mixture were determined from phase equilibrium measurements [46,48,49,51], high-pressure optical phase equilibrium cell [47], and from *PVTx* measurements using a metal-bellows variable volumeter with an optical cell [50]. The agreement between different sources is good (see Sect. 3.3), except for the data reported by Rizvi and Heidemann [46] and Gillespie et al. [51] for the critical pressure. Very limited (three data points by Sakabe et al. [50]) experimental critical density data are available in the literature. These data together with the present values of the critical parameters were used to calculate the Krichevskii parameter (see Sect. 4.1) for this mixture.

2 Experimental

2.1 Isochoric Heat-Capacity Apparatus

The experimental details (physical basis and the theory of the method, the apparatus, procedures of the measurements, and the uncertainty assessment) of the isochoric heat-capacity measurements have been described in our earlier publications [52–64]. Therefore, only essential information will be given here. Isochoric heat-capacity ($C_V VTx$) measurements were performed with a high-temperature, high-pressure, nearly constant-volume adiabatic calorimeter. The physical basis of the method is as follows: if a layer of a semiconductor (Cu_2O) is placed between two concentric spherical vessels, then the system will behave as a highly sensitive thermoelement that can serve as a sensor detecting deviations from adiabatic conditions. Since cuprous oxide (Cu_2O) has a very high thermoelectric power α (about $1150\,\mu V \cdot K^{-1}$), the adiabatic conditions are reliably maintained in this calorimeter [52,53]. This makes it possible to detect extremely small temperature differences (10^{-6} K) between the inner and outer spherical vessels and to eliminate possible heat transfer through the semiconductor layer. Therefore, the heat that is released by the micro-heater located in the calorimeter is used only to heat the fluid located inside the inner thin-walled shell of the calorimeter and a thin layer of Cu_2O that directly adjoins the inner shell. Since Cu_2O has a small thermal conductivity ($\lambda \approx 2.09\ W \cdot m^{-1} \cdot K^{-1}$), use of this semiconductor leads only to negligibly small heat losses. The out-of-balance signal from the integrating thermoelement (Cu_2O) is applied first to the input of an amplifying microvoltmeter whose output feeds a high-precision temperature regulator (HPTR).

The heat capacity is obtained from measurements of the following quantities: mass of the fluid, m; electrical energy released by the inner heater, ΔQ; temperature change,

ΔT, resulting from the addition of the energy ΔQ; and the empty calorimeter heat capacity, C_0. The final working equation for this method is

$$C_V = \frac{1}{m}\left\{\frac{\Delta Q}{\Delta T} - C_0\right\}. \tag{1}$$

When measurements are made near the critical point, the sample is vigorously mixed by a stirrer made of a thin perforated foil of stainless steel.

The temperature was measured with a PRT-10. The uncertainty in the temperature measurements was 15 mK. Based on a detailed analysis of all the sources [52,53] of uncertainties, which are likely to affect the determination of C_V, the expanded uncertainty (a coverage factor $k = 2$ and thus a two-standard-deviation estimate) of measuring the heat capacity was 2 % to 3 % in the near-critical and supercritical regions, 1.0 % to 1.5 % in the liquid phase, and 3 % to 4 % in the vapor phase. The uncertainty in density measurements was 0.05 %.

The heat capacity was measured as a function of temperature at a nearly constant density. The calorimeter was filled at room temperature, sealed off, and heated along a quasi-isochore. Each run for the heat capacity was normally started in the two-phase (L–V) region and completed in the single-phase region. Between initial (L–V) and final (liquid or vapor phase, depending on the filling factor) phase states, the system passed through the liquid–gas phase transition temperature. This method enables one to determine the transition temperature T_S, the jump in the heat capacity ΔC_V, and reliable C_V data in the single- and two-phase regions for each quasi-isochore with an uncertainty of 0.02 K, [52–65]. The single- and two-phase vapor (C''_{V1}, C''_{V2}) and liquid (C'_{V1}, C'_{V2},) heat capacities at saturation, the saturated temperature (T_S), and saturated liquid (ρ'_S) and vapor (ρ''_S) densities can also be measured for near-critical fluids with this method as discussed below.

2.2 Quasi-Static Thermograms Technique

The method of quasi-static thermograms (temperature versus time, T–τ plot) was used to precisely determine the location of the phase transition, the liquid–vapor boundary (T_S, ρ'_S, ρ''_S) coordinates near the critical point and the critical parameters (T_C, ρ_C) for $NH_3 + H_2O$ mixtures. The details and basic idea of the method of quasi-static thermograms and its application to complex thermodynamic systems (with solid–liquid, liquid–liquid, liquid–gas, liquid–liquid–gas, solid–liquid–gas, and solid–liquid–liquid phase transitions) are described in our previous publications [53–55,64,65]. Synchronous recording of the resistance thermometer (T–τ plot) and of the sensor of adiabatic control readings follows the thermodynamic state of the sample as it approaches the phase transition point. On intersecting the liquid–vapor phase transition point, the heat capacity is known to change discontinuously, leading to a sharp change in the thermogram slope, $dT/d\tau$. The magnitude of the thermogram slope changes is proportional to the heat capacity jump,

$$\Delta C_V = k\left[\left(\frac{\mathrm{d}\tau}{\mathrm{d}T}\right)_{VT_S-0} - \left(\frac{\mathrm{d}\tau}{\mathrm{d}T}\right)_{VT_S+0}\right]. \tag{2}$$

Here, $\left(\frac{\mathrm{d}\tau}{\mathrm{d}T}\right)_{VT_S-0}$ and $\left(\frac{\mathrm{d}\tau}{\mathrm{d}T}\right)_{VT_S+0}$ are the slopes of the thermograms before and after the phase transition point T_S, respectively; k is a coefficient depending on the power of the heat flow and the mass of the sample studied; and T_S is the temperature of the phase transition corresponding to the fixed isochore V. It is well known [66,67] that the isochoric heat-capacity jump ΔC_V diverges at the critical point as $\Delta C_V \propto (T - T_C)^{-\alpha}$, where $\alpha = 0.112$ is the universal critical exponent. Therefore, the difference $\left[\left(\frac{\mathrm{d}\tau}{\mathrm{d}T}\right)_{VT_S-0} - \left(\frac{\mathrm{d}\tau}{\mathrm{d}T}\right)_{VT_S+0}\right]$ between the thermogram slopes before and after the phase transition point in the critical region is very large (diverging at the critical point). This makes it easy to detect any type of phase transitions occurring in the system near the phase transition and the critical points. Therefore, quasi-static thermogram methods allow accurate determination of the phase-boundary properties near the critical point. If the critical density of the fluid is known (heating calorimetric vessel with the critical filling densities), the values of the critical temperature and the critical pressure can be measured very accurately (within 0.02 K and 0.05 %, respectively). In order to determine the value of the critical density by this method, the series of isochores can be measured around the expected critical density, and then the value of the critical density can be accurately extracted by analytically evaluating the $T_S - \rho_S$ data in the immediate vicinity of the critical point. This method of determination of the phase transition and critical points has certain advantages over other methods (for example, the visual method). In particular, it has a low uncertainty and high reliability.

The most widely used experimental method of determining the parameters of the coexistence curve by visually observing the disappearance of the meniscus lacks objectivity. Moreover, on approaching the critical point, where the difference between the liquid and vapor phases vanishes, the visual determination of the moment at which the phase transition occurs becomes ever less reliable. In addition, the observations are impeded by the development of critical opalescence. Therefore, the region of temperatures near the critical point (within 1 K of T_c) becomes virtually unattainable for investigation.

The method under consideration makes it possible to obtain reliable data within 0.02 K of T_c. This technique of determining phase boundary parameters (T_S, ρ'_S, ρ''_S) is similar to the method of quasi-static thermograms described by Chashkin et al. [68] and Vorornel [69]. However, in comparison with the method described in Refs. [68] and [69], the method of quasi-static thermograms here is supplemented by recording the readings of the adiabatic control sensor. In combination (quasi-static thermograms, T–τ plot, and the adiabatic control), these ensure sufficient information on the changes in the sample thermodynamic state (for example, the presence of any temperature gradient in the volume of the sample) in different places inside the calorimeter (in the middle and near the inner surface of the inner calorimetric vessel). This is a very accurate technique to determine the phase changes in complicated multicomponent mixtures where it is difficult to determine the number of phase changes at constant volume heating [55,65]. Any jumps in a C_V–T plot or thermogram (T–τ plot) breaks means that the number of phases in the system has changed, increasing or decreasing,

depending on increasing or decreasing the values of C_V after the phase transition occurs.

In order to check the accuracy of the method and confirm the reliability of phase transitions and critical-point parameter determination by the quasi-static thermogram technique, the method was applied for three standard fluids (pure distilled light and heavy water, and high purity toluene). The measured values of phase transition temperatures, $T_S = (647.104 \pm 0.02)$ K (light water) and $T_S = (643.83 \pm 0.02)$ K (heavy water), for near-critical filling densities of 321.96 kg · m^{-3} ($\rho_C = 322.0$ kg · m^{-3}, the critical density of light water accepted by IAPWS [70]) and 356.8 kg · m^{-3} ($\rho_C = 356.0$ kg · m^{-3}, the critical density of heavy water accepted by IAPWS [71]), respectively, for light and heavy water, are in very close agreement with the critical temperatures $T_C = 647.096$ K and $T_C = 643.847$ K adopted by IAPWS for pure light [70] and heavy water [71]. The deviations for the two measurements of 8 mK and 13 mK are within our uncertainty (20 mK). Our results for the critical temperature $T_C = (591.89 \pm 0.02)$ K and the critical density $\rho_C = (291.6 \pm 2)$ kg · m^{-3} for toluene are in good agreement (within 0.006 K to 0.174 K for the critical temperature and 0.02 kg · m^{-3} to 0.6 kg · m^{-3} for the critical density) with the reported values by other authors (deviation within 0.4 K is found between the present critical temperature and the values recommended by other authors [72–75]). This is still within the estimated uncertainty (0.6 K) claimed by the authors.

The 0.2607 NH_3 + 0.7393 H_2O mixture was prepared by a commercial supplier. The uncertainty in the concentration provided by the supplier is 5×10^{-5} mole fraction.

3 Results and Discussion

Measurements of the single- and two-phase isochoric heat capacities of 0.2607 $NH_3 + 0.7393 H_2O$ mixture were performed along 38 liquid and vapor isochores from 120 kg · m^{-3} to 671 kg · m^{-3} as a function of temperature in the range from 478 K to 634 K. Most measurements were made in a range of temperatures in the immediate vicinity of the phase transition and critical points for each isochore to precisely determine the phase boundary properties (T_S, ρ'_S, ρ''_S) and the critical parameters. Detailed measurements of the phase transition boundary allowed precise determination of the shape of the saturation curve near the critical point and accurate determination the critical parameters (T_C and ρ_C). The experimental temperature, density, and single- and two-phase isochoric heat-capacity values for 0.2603 $NH_3 + 0.7397$ H_2O mixture are presented in Table 1. Some selected experimental results are shown in Figs. 1, 2, 3, 4, 5 in $C_V - T$ and $C_V - \rho$ projections, together with values calculated from the multiparametric EOS by Tillner-Roth and Friend [28] and crossover model by Kiselev and Rainwater [29]. The measured values of the isochoric heat capacities along the liquid isochores are systematically higher than the calculated values by 12 %, while for vapor isochores, the deviations are within 9 %. The crossover model-predicted values of the isochoric heat capacity agree only qualitatively with the present results.

Table 1 Experimental values of the single- and two-phase isochoric heat capacities of $NH_3 + H_2O$ mixture ($x = 0.2607$ mole fraction of NH_3)

$\rho = 671.23\,\mathrm{kg \cdot m^{-3}}$		$\rho = 649.65\,\mathrm{kg \cdot m^{-3}}$		$\rho = 594.32\,\mathrm{kg \cdot m^{-3}}$	
T (K)	C_{VX} $(\mathrm{kJ \cdot kg^{-1} \cdot K^{-1}})$	T (K)	C_{VX} $(\mathrm{kJ \cdot kg^{-1} \cdot K^{-1}})$	T (K)	C_{VX} $(\mathrm{kJ \cdot kg^{-1} \cdot K^{-1}})$
477.99	5.318	509.39	5.502	530.70	5.906
477.18	5.358	509.67	5.537	530.79	5.852
478.28	5.352	509.77	5.493	530.88	5.833
478.37	5.361	509.95	5.505	530.98	5.822
477.18	5.358	514.27	5.564	531.16	5.910
478.28	5.352	514.45	5.554	531.25	5.877
478.37	5.361	514.64	5.568	534.24	5.897
478.57	5.325	514.73	5.525	534.43	5.852
484.75	5.411	519.21	5.558	534.56	5.913
484.94	5.414	519.31	5.586	534.75	5.946
485.04	5.407	519.59	5.571	534.84	5.898
485.23	5.400	519.68	5.620	539.24	5.886
485.33	5.425	519.77	5.607	539.42	5.901
492.43	5.475	519.77	3.875	539.51	5.935
492.62	5.496	519.87	3.842	539.60	5.814
492.71	5.473	520.05	3.716	539.79	6.046
492.91	5.478	520.14	3.768	539.88	5.954
498.43	5.509	520.24	3.788	539.97	6.057
498.53	5.528	520.33	3.653	541.79	5.943
498.62	5.497	520.42	3.752	541.89	5.901
498.71	5.513	520.52	3.778	541.98	5.885
498.81	5.556	520.79	3.709	542.07	5.907
498.90	5.494	520.98	3.682	542.16	5.995
506.85	5.524	521.17	3.767	542.25	5.875
506.94	5.548	521.35	3.757	542.34	5.898
507.04	5.572	521.45	3.720	542.43	5.958
507.13	5.569	521.54	3.706	542.52	5.889
507.32	5.554	526.45	3.595	544.89	5.912
507.41	5.596	526.64	3.589	544.98	5.988
507.51	5.601	526.82	3.572	545.07	6.073
507.70	5.570	527.01	3.584	545.17	6.034
507.79	5.564	527.19	3.538	545.26	6.012
507.98	5.501	527.28	3.568	545.35	5.974
508.07	5.456	–	–	545.44	6.034
508.07	3.843	–	–	545.53	5.951
508.26	3.837	–	–	545.62	5.971
508.36	3.850	–	–	545.62	4.015
508.45	3.803	–	–	545.71	3.922
508.54	3.807	–	–	545.80	3.894
508.64	3.783	–	–	546.08	3.855
509.01	3.856	–	–	546.17	3.800
509.11	3.812	–	–	546.35	3.856
509.30	3.823	–	–	546.62	3.781
509.39	3.758	–	–	546.71	3.743
509.67	3.778	–	–	547.07	3.695
513.42	3.690	–	–	547.17	3.735
513.61	3.663	–	–	547.50	3.690
513.80	3.694	–	–	547.79	3.686
516.88	3.578	–	–	547.98	3.599

Table 1 continued

$\rho = 671.23\,\mathrm{kg \cdot m^{-3}}$		$\rho = 649.65\,\mathrm{kg \cdot m^{-3}}$		$\rho = 594.32\,\mathrm{kg \cdot m^{-3}}$	
T (K)	C_{VX} $\left(\mathrm{kJ \cdot kg^{-1} \cdot K^{-1}}\right)$	T (K)	C_{VX} $\left(\mathrm{kJ \cdot kg^{-1} \cdot K^{-1}}\right)$	T (K)	C_{VX} $\left(\mathrm{kJ \cdot kg^{-1} \cdot K^{-1}}\right)$
517.07	3.556	–	–	549.80	3.591
517.26	3.551	–	–	549.98	3.546
517.44	3.563	–	–	550.07	3.589
517.63	3.516	–	–	550.16	3.573
517.82	3.575	–	–	550.34	3.579
$\rho = 552.58\,\mathrm{kg \cdot m^{-3}}$		$\rho = 476.25\,\mathrm{kg \cdot m^{-3}}$		$\rho = 456.58\,\mathrm{kg \cdot m^{-3}}$	
T (K)	C_{VX} $\left(\mathrm{kJ \cdot kg^{-1} \cdot K^{-1}}\right)$	T (K)	C_{VX} $\left(\mathrm{kJ \cdot kg^{-1} \cdot K^{-1}}\right)$	T (K)	C_{VX} $\left(\mathrm{kJ \cdot kg^{-1} \cdot K^{-1}}\right)$
530.61	5.559	530.70	5.701	541.89	5.790
530.75	5.568	530.84	5.643	552.81	6.029
530.93	5.594	530.98	5.604	552.99	6.101
531.16	5.534	531.16	5.648	553.34	6.109
531.30	5.578	540.15	5.807	556.72	6.270
539.97	5.762	540.43	5.843	556.81	6.260
540.06	5.719	540.61	5.905	556.99	6.210
540.15	5.653	540.79	5.826	557.26	6.220
540.24	5.704	548.07	6.104	568.56	6.870
540.33	5.752	548.25	6.135	571.09	7.005
540.43	5.753	548.44	6.198	571.64	7.085
540.52	5.705	548.71	6.143	572.25	7.039
550.88	5.986	559.09	6.588	578.55	7.326
550.52	5.923	559.27	6.419	579.85	7.328
550.15	5.981	559.36	6.502	579.77	7.398
551.25	5.947	559.45	6.470	580.03	7.350
551.34	5.978	559.63	6.409	581.42	7.458
551.43	5.930	569.83	6.908	581.51	7.511
551.52	5.890	570.12	6.953	581.77	7.484
554.59	6.074	570.81	6.794	581.86	7.513
554.68	6.020	570.90	6.885	582.03	7.486
554.77	6.096	570.99	6.822	582.12	7.536
554.86	6.073	575.01	7.073	583.42	7.552
554.95	6.037	575.17	7.044	583.55	7.644
555.04	6.104	575.30	7.061	583.68	7.608
555.13	6.145	575.01	7.073	583.77	7.626
559.27	6.335	575.17	7.044	583.94	7.632
559.36	6.306	575.30	7.061	584.74	7.724
559.45	6.318	575.52	7.029	584.72	7.743
559.54	6.327	575.70	7.038	584.90	7.749
559.63	6.311	575.83	7.071	584.95	7.760
559.81	6.336	579.68	7.218	584.95	4.620
559.90	6.363	579.61	7.181	584.98	4.560
559.99	6.353	579.86	7.155	585.16	4.537
560.49	6.317	579.99	7.268	585.42	4.499
560.66	6.318	580.12	7.281	585.50	4.520
560.80	6.345	580.18	7.237	585.68	4.408
560.89	6.379	580.18	4.350	587.06	4.246
560.98	6.326	580.21	4.145	587.06	4.246
561.03	6.367	580.30	3.927	587.24	4.278

Table 1 continued

$\rho = 552.58\,\mathrm{kg \cdot m^{-3}}$		$\rho = 476.25\,\mathrm{kg \cdot m^{-3}}$		$\rho = 456.58\,\mathrm{kg \cdot m^{-3}}$	
T (K)	C_{VX} $\left(\mathrm{kJ \cdot kg^{-1} \cdot K^{-1}}\right)$	T (K)	C_{VX} $\left(\mathrm{kJ \cdot kg^{-1} \cdot K^{-1}}\right)$	T (K)	C_{VX} $\left(\mathrm{kJ \cdot kg^{-1} \cdot K^{-1}}\right)$
561.03	4.122	580.56	3.853	587.41	4.241
561.19	3.983	580.74	3.855	587.50	4.193
561.25	3.756	580.92	3.820	587.58	4.290
561.34	3.649	581.01	3.856	595.10	3.991
561.52	3.607	580.92	3.820	595.18	3.948
561.61	3.516	581.01	3.856	595.35	4.005
561.70	3.626	581.09	3.813	595.44	3.872
561.88	3.561	581.18	3.792	595.53	4.017
561.97	3.536	581.36	3.732	595.61	3.859
562.06	3.459	581.54	3.759	595.70	3.996
–	–	581.62	3.721	599.31	3.791
–	–	584.62	3.706	599.48	3.766
–	–	584.71	3.661	599.65	3.742
–	–	584.80	3.640	599.82	3.765
–	–	584.88	3.678	602.48	3.728
–	–	584.97	3.675	602.65	3.860
–	–	585.15	3.639	602.82	3.804
$\rho = 376.89\,\mathrm{kg \cdot m^{-3}}$		$\rho = 342.18\,\mathrm{kg \cdot m^{-3}}$		$\rho = 329.00\,\mathrm{kg \cdot m^{-3}}$	
T (K)	C_{VX} $\left(\mathrm{kJ \cdot kg^{-1} \cdot K^{-1}}\right)$	T (K)	C_{VX} $\left(\mathrm{kJ \cdot kg^{-1} \cdot K^{-1}}\right)$	T (K)	C_{VX} $\left(\mathrm{kJ \cdot kg^{-1} \cdot K^{-1}}\right)$
553.70	6.133	563.36	6.461	580.68	7.646
571.02	6.892	563.54	6.629	580.54	7.641
590.78	8.872	563.63	6.544	580.99	7.488
591.22	9.335	563.72	6.440	581.07	7.611
591.73	9.066	563.81	6.501	581.16	7.612
593.93	9.696	563.98	6.597	590.87	8.561
594.06	9.733	581.42	7.895	591.01	8.581
594.15	9.632	581.51	7.835	591.13	8.591
594.23	9.702	581.59	8.016	591.22	8.442
594.32	9.951	581.77	7.889	591.30	8.530
594.58	10.15	581.86	8.030	591.39	8.461
594.71	9.981	590.05	8.739	597.76	11.65
594.84	10.06	590.18	8.704	597.85	11.51
594.92	9.891	590.35	8.847	597.93	11.57
595.01	10.03	590.52	8.955	598.02	11.65
595.10	9.830	595.35	9.999	598.11	11.89
595.16	10.04	595.44	10.12	598.19	11.75
595.16	5.580	595.59	10.02	598.28	12.19
595.18	5.453	595.70	10.26	598.33	12.18
595.27	5.380	595.87	10.24	598.33	6.610
595.44	5.410	596.82	10.61	598.45	6.375
595.53	5.220	596.90	10.53	598.54	6.170
595.61	5.341	596.99	10.61	598.71	5.787
595.78	5.037	597.08	10.71	599.05	6.048
595.87	5.134	597.20	10.56	599.22	5.647
595.96	4.980	597.33	10.76	599.31	5.473
595.78	5.037	597.46	11.03	605.13	4.836
595.87	5.134	597.56	11.19	605.22	4.968

Table 1 continued

$\rho = 376.89\,\mathrm{kg \cdot m^{-3}}$		$\rho = 342.18\,\mathrm{kg \cdot m^{-3}}$		$\rho = 329.00\,\mathrm{kg \cdot m^{-3}}$	
T (K)	C_{VX} $\left(\mathrm{kJ \cdot kg^{-1} \cdot K^{-1}}\right)$	T (K)	C_{VX} $\left(\mathrm{kJ \cdot kg^{-1} \cdot K^{-1}}\right)$	T (K)	C_{VX} $\left(\mathrm{kJ \cdot kg^{-1} \cdot K^{-1}}\right)$
595.96	4.980	597.56	6.250	605.30	4.640
597.16	4.950	597.59	6.008	605.39	4.715
597.50	4.840	597.67	5.692	605.56	4.739
597.68	4.971	597.76	5.272	616.24	4.454
597.93	4.641	597.85	5.582	616.45	4.249
598.28	4.707	597.93	5.312	616.54	4.345
598.97	4.593	598.02	5.238	616.62	4.295
601.88	4.450	600.90	5.002	616.71	4.323
601.97	4.318	601.02	4.923	–	–
602.05	4.510	601.24	5.002	–	–
602.48	4.573	601.37	5.030	–	–
602.65	4.566	602.48	4.874	–	–
602.74	4.465	602.56	4.919	–	–
606.41	4.534	602.74	4.923	–	–
606.58	4.588	602.91	4.668	–	–
606.67	4.676	602.99	4.781	–	–
606.76	4.622	607.69	4.300	–	–
606.84	4.487	607.78	4.567	–	–
607.86	4.468	607.86	4.424	–	–
607.95	4.519	607.95	4.282	–	–
608.04	4.441	612.29	4.405	–	–
608.12	4.338	612.55	4.348	–	–
608.21	4.275	612.63	4.432	–	–
608.29	4.472	612.80	4.407	–	–
608.38	4.290	618.23	4.397	–	–
612.46	4.302	618.32	4.363	–	–
612.55	4.420	618.50	4.409	–	–
612.63	4.214	618.57	4.420	–	–
612.80	4.256	618.66	4.323	–	–
612.89	4.364	–	–	–	–
$\rho = 320.33\,\mathrm{kg \cdot m^{-3}}$		$\rho = 312.91\,\mathrm{kg \cdot m^{-3}}$		$\rho = 311.19\,\mathrm{kg \cdot m^{-3}}$	
T (K)	C_{VX} $\left(\mathrm{kJ \cdot kg^{-1} \cdot K^{-1}}\right)$	T (K)	C_{VX} $\left(\mathrm{kJ \cdot kg^{-1} \cdot K^{-1}}\right)$	T (K)	C_{VX} $\left(\mathrm{kJ \cdot kg^{-1} \cdot K^{-1}}\right)$
581.42	7.658	582.38	7.602	593.46	8.690
581.51	7.468	582.46	7.643	593.54	8.660
581.68	7.510	582.55	7.625	593.63	8.362
581.77	7.476	582.64	7.684	593.72	9.027
581.94	7.340	582.72	7.429	593.80	8.552
591.30	8.927	582.81	7.429	597.07	9.939
591.47	8.894	582.90	7.450	597.16	10.21
591.56	8.734	591.82	8.484	597.25	10.45
591.65	8.620	591.91	8.583	597.42	10.27
591.73	8.999	591.99	8.538	597.50	9.909
598.36	11.72	592.08	8.750	597.59	10.25
598.45	11.60	592.16	8.371	598.97	11.18
598.53	12.09	592.25	8.313	599.05	11.56
598.62	11.93	598.88	11.54	599.14	11.38
598.71	12.21	598.96	11.03	599.22	11.82

Table 1 continued

$\rho = 320.33\,\mathrm{kg \cdot m^{-3}}$		$\rho = 312.91\,\mathrm{kg \cdot m^{-3}}$		$\rho = 311.19\,\mathrm{kg \cdot m^{-3}}$	
T (K)	C_{VX} $\left(\mathrm{kJ \cdot kg^{-1} \cdot K^{-1}}\right)$	T (K)	C_{VX} $\left(\mathrm{kJ \cdot kg^{-1} \cdot K^{-1}}\right)$	T (K)	C_{VX} $\left(\mathrm{kJ \cdot kg^{-1} \cdot K^{-1}}\right)$
598.79	12.31	599.05	11.04	599.31	11.97
598.88	12.69	599.14	11.57	599.39	12.40
598.96	12.86	599.22	11.86	599.48	13.24
598.96	6.802	599.31	12.52	599.54	13.42
599.05	6.705	599.36	13.16	599.57	13.53
599.14	6.566	599.42	13.25	599.57	7.060
599.22	6.559	599.42	6.990	599.63	6.584
599.31	6.432	599.48	6.560	599.74	6.743
599.39	6.585	599.57	6.077	599.82	6.427
600.94	5.343	599.65	5.563	602.91	5.096
601.02	5.403	599.74	5.379	602.99	5.218
601.11	5.071	599.99	5.153	603.08	4.970
601.19	5.000	602.14	4.682	603.16	4.899
601.28	5.126	602.22	4.663	603.25	5.060
601.47	5.220	602.30	4.567	603.42	4.990
609.40	4.923	602.39	4.602	610.42	4.753
609.48	4.745	602.48	4.769	610.51	4.564
609.57	4.841	610.17	4.732	610.53	4.627
609.65	4.544	610.25	4.675	610.77	4.505
609.74	4.698	610.33	4.617	610.84	4.641
–	–	610.42	4.600	615.86	4.538
–	–	610.51	4.609	615.94	4.632
–	–	610.59	4.548	616.03	4.407
–	–	615.94	4.738	616.20	4.453
–	–	616.03	4.596	616.37	4.395
–	–	616.20	4.399	–	–
–	–	616.29	4.344	–	–
–	–	616.37	4.544	–	–
$\rho = 309.95\,\mathrm{kg \cdot m^{-3}}$		$\rho = 308.35\,\mathrm{kg \cdot m^{-3}}$		$\rho = 307.35\,\mathrm{kg \cdot m^{-3}}$	
T (K)	C_{VX} $\left(\mathrm{kJ \cdot kg^{-1} \cdot K^{-1}}\right)$	T (K)	C_{VX} $\left(\mathrm{kJ \cdot kg^{-1} \cdot K^{-1}}\right)$	T (K)	C_{VX} $\left(\mathrm{kJ \cdot kg^{-1} \cdot K^{-1}}\right)$
590.67	8.356	582.29	7.376	582.29	7.239
590.70	8.615	582.38	7.165	582.37	7.096
590.78	8.584	582.46	7.282	582.47	7.243
590.87	8.680	582.55	6.938	582.56	7.269
590.96	8.492	582.64	7.197	582.63	7.150
595.52	9.752	582.72	7.085	582.73	7.393
595.61	9.884	590.78	8.218	592.51	8.952
595.69	9.584	590.96	8.020	592.60	8.653
595.79	9.823	591.04	8.328	592.68	8.731
595.87	9.543	591.13	8.172	592.77	8.487
595.99	9.991	591.21	7.982	592.85	8.786
596.12	9.772	591.30	8.169	592.94	8.620
599.05	11.71	591.39	8.265	596.39	10.15
599.13	11.56	596.26	10.27	596.47	10.08
599.23	11.65	596.39	10.32	596.55	10.27
599.30	11.86	596.47	10.04	596.64	10.12
599.39	12.30	596.56	10.27	596.71	10.10

Table 1 continued

$\rho = 309.95\,\mathrm{kg \cdot m^{-3}}$		$\rho = 308.35\,\mathrm{kg \cdot m^{-3}}$		$\rho = 307.35\,\mathrm{kg \cdot m^{-3}}$	
T (K)	C_{VX} $\left(\mathrm{kJ \cdot kg^{-1} \cdot K^{-1}}\right)$	T (K)	C_{VX} $\left(\mathrm{kJ \cdot kg^{-1} \cdot K^{-1}}\right)$	T (K)	C_{VX} $\left(\mathrm{kJ \cdot kg^{-1} \cdot K^{-1}}\right)$
599.48	12.14	596.64	10.42	596.91	10.07
599.56	13.44	596.73	10.35	596.98	10.07
599.62	13.70	599.22	11.90	599.31	11.45
599.67	13.84	599.31	11.65	599.40	11.92
599.67	7.110	599.39	11.49	599.48	11.59
599.74	6.921	599.48	11.24	599.57	11.91
599.78	6.780	599.57	11.65	599.66	12.91
599.82	6.223	599.65	12.37	599.73	13.03
599.91	5.867	599.74	13.29	599.83	13.47
599.99	5.776	599.78	13.71	599.89	13.51
600.35	5.632	599.78	6.990	599.89	6.820
600.42	5.586	599.91	6.622	599.99	6.598
600.51	5.675	599.99	5.962	600.08	5.819
600.59	5.686	600.08	5.686	600.16	5.691
600.69	5.377	600.17	5.273	602.13	5.458
607.78	4.702	600.45	5.346	602.23	5.202
607.87	4.553	600.62	5.126	602.40	5.316
607.95	4.867	600.80	5.218	602.48	5.032
608.04	4.673	600.98	5.022	602.56	5.191
608.21	4.743	609.65	4.328	610.59	4.721
616.20	4.612	609.82	4.207	610.68	4.708
616.28	4.576	609.91	4.430	610.76	4.792
616.37	4.533	609.99	4.382	610.85	4.613
616.45	4.427	610.08	4.323	610.93	4.552
616.55	4.670	–	–	611.02	4.697
–	–	–	–	611.10	4.576
$\rho = 305.44\,\mathrm{kg \cdot m^{-3}}$		$\rho = 303.47\,\mathrm{kg \cdot m^{-3}}$		$\rho = 301.94\,\mathrm{kg \cdot m^{-3}}$	
T (K)	C_{VX} $\left(\mathrm{kJ \cdot kg^{-1} \cdot K^{-1}}\right)$	T (K)	C_{VX} $\left(\mathrm{kJ \cdot kg^{-1} \cdot K^{-1}}\right)$	T (K)	C_{VX} $\left(\mathrm{kJ \cdot kg^{-1} \cdot K^{-1}}\right)$
589.49	8.186	589.92	8.100	590.96	8.725
589.57	8.147	590.01	8.078	591.04	8.679
589.66	8.317	590.09	8.358	591.13	8.466
589.75	8.237	590.18	8.216	591.22	8.683
589.83	8.131	590.31	8.338	591.34	8.589
589.92	8.194	599.50	11.25	599.31	10.96
590.01	8.027	599.64	11.52	599.44	11.16
599.48	11.42	599.74	11.70	599.57	10.94
599.57	11.40	599.82	11.44	599.65	10.72
599.65	11.63	599.91	11.54	599.74	11.20
599.74	11.55	599.99	12.13	599.82	11.10
599.82	12.12	600.09	12.47	599.99	12.39
599.91	12.87	600.16	12.89	600.08	12.16
599.99	13.33	600.17	13.24	600.17	12.77
600.02	13.38	600.17	6.630	600.25	12.52
600.02	6.730	600.25	6.222	600.29	13.15
600.08	6.540	600.34	5.857	600.29	6.620
600.17	6.073	600.42	5.568	600.33	6.290
600.25	5.774	600.50	5.324	600.43	6.112

Table 1 continued

$\rho = 305.44\,\mathrm{kg \cdot m^{-3}}$		$\rho = 303.47\,\mathrm{kg \cdot m^{-3}}$		$\rho = 301.94\,\mathrm{kg \cdot m^{-3}}$	
T (K)	C_{VX} $\left(\mathrm{kJ \cdot kg^{-1} \cdot K^{-1}}\right)$	T (K)	C_{VX} $\left(\mathrm{kJ \cdot kg^{-1} \cdot K^{-1}}\right)$	T (K)	C_{VX} $\left(\mathrm{kJ \cdot kg^{-1} \cdot K^{-1}}\right)$
600.34	5.920	600.59	5.316	600.51	5.968
600.42	5.513	600.66	5.357	600.59	5.613
600.77	5.732	–	–	601.11	5.483
600.85	5.413	–	–	601.19	5.316
600.94	5.625	–	–	601.29	5.528
601.02	5.599	–	–	601.34	5.389
601.11	5.355	–	–	601.45	5.209
601.19	5.322	–	–	601.54	5.269
–	–	–	–	611.02	4.826
–	–	–	–	611.10	4.864
–	–	–	–	611.23	4.769
–	–	–	–	611.35	4.683
–	–	–	–	611.44	4.695
–	–	–	–	611.61	4.794
$\rho = 299.79\,\mathrm{kg \cdot m^{-3}}$		$\rho = 297.60\,\mathrm{kg \cdot m^{-3}}$		$\rho = 294.44\,\mathrm{kg \cdot m^{-3}}$	
T (K)	C_{VX} $\left(\mathrm{kJ \cdot kg^{-1} \cdot K^{-1}}\right)$	T (K)	C_{VX} $\left(\mathrm{kJ \cdot kg^{-1} \cdot K^{-1}}\right)$	T (K)	C_{VX} $\left(\mathrm{kJ \cdot kg^{-1} \cdot K^{-1}}\right)$
591.22	8.498	589.75	8.736	597.12	9.715
591.34	8.502	589.83	8.867	597.25	9.872
591.47	8.319	589.92	8.641	597.33	9.641
591.56	8.725	590.01	8.831	597.42	9.901
591.69	8.471	590.09	8.612	597.50	9.804
598.79	10.88	590.18	8.688	597.63	9.956
598.88	11.03	598.23	10.37	599.74	10.82
599.01	10.86	598.41	10.16	599.82	10.88
599.18	10.75	598.58	10.23	599.91	11.03
599.31	10.90	598.75	10.48	600.02	11.03
600.17	11.69	600.34	12.66	600.17	11.31
600.25	12.24	600.42	12.82	599.74	10.82
600.34	12.77	600.51	12.88	599.82	10.88
600.42	12.38	600.59	12.80	599.91	11.03
600.48	13.04	600.63	12.78	600.02	11.03
600.48	6.570	600.63	6.470	600.17	11.31
600.50	6.340	600.72	6.343	600.77	12.38
600.59	5.898	600.77	6.179	600.81	12.64
600.67	5.714	600.85	5.943	600.81	6.410
600.77	5.556	600.94	5.846	600.85	6.272
600.86	5.606	601.37	5.791	600.94	5.851
601.46	5.462	601.45	5.612	601.37	5.942
601.53	5.575	601.54	5.700	601.45	5.767
601.63	5.543	601.97	5.648	601.66	5.630
601.71	5.357	619.76	4.294	601.82	5.560
611.19	4.605	619.93	4.229	609.48	5.134
611.27	4.623	620.01	4.372	609.57	5.027
611.36	4.522	620.10	4.326	609.65	4.939
611.44	4.593	–	–	609.74	5.064
611.53	4.558	–	–	609.82	5.013
611.61	4.497	–	–	–	–

Table 1 continued

$\rho = 299.79\,\mathrm{kg \cdot m^{-3}}$		$\rho = 297.60\,\mathrm{kg \cdot m^{-3}}$		$\rho = 294.44\,\mathrm{kg \cdot m^{-3}}$	
T (K)	C_{VX} $\left(\mathrm{kJ \cdot kg^{-1} \cdot K^{-1}}\right)$	T (K)	C_{VX} $\left(\mathrm{kJ \cdot kg^{-1} \cdot K^{-1}}\right)$	T (K)	C_{VX} $\left(\mathrm{kJ \cdot kg^{-1} \cdot K^{-1}}\right)$
616.69	4.634	–	–	–	–
616.84	4.524	–	–	–	–
616.95	4.584	–	–	–	–
617.05	4.625	–	–	–	–
617.13	4.504	–	–	–	–
617.31	4.533	–	–	–	–
617.46	4.557	–	–	–	–
$\rho = 292.97\,\mathrm{kg \cdot m^{-3}}$		$\rho = 291.16\,\mathrm{kg \cdot m^{-3}}$		$\rho = 285.71\,\mathrm{kg \cdot m^{-3}}$	
T (K)	C_{VX} $\left(\mathrm{kJ \cdot kg^{-1} \cdot K^{-1}}\right)$	T (K)	C_{VX} $\left(\mathrm{kJ \cdot kg^{-1} \cdot K^{-1}}\right)$	T (K)	C_{VX} $\left(\mathrm{kJ \cdot kg^{-1} \cdot K^{-1}}\right)$
597.68	9.188	598.36	9.836	595.44	8.219
597.76	9.147	598.49	9.943	595.53	8.365
597.85	9.034	598.62	9.901	595.61	8.081
597.93	9.391	598.71	10.11	595.78	8.447
598.02	9.297	598.79	9.922	595.87	8.281
598.11	9.411	598.88	10.15	600.68	10.46
600.67	12.34	600.51	11.24	600.81	10.72
600.75	12.44	600.64	11.19	600.94	10.82
600.86	12.24	600.77	11.33	601.07	10.87
600.93	12.45	600.85	11.67	601.19	11.07
600.93	6.310	600.93	11.78	601.28	11.25
600.94	5.972	600.98	11.89	601.34	11.51
601.04	5.729	601.02	11.70	601.34	6.080
601.11	5.317	601.05	12.03	601.37	5.608
601.21	5.616	601.05	6.270	601.45	5.318
–	–	601.08	5.919	601.54	5.024
–	–	601.12	5.260	601.62	5.006
–	–	601.21	5.330	601.71	4.953
–	–	601.39	5.193	–	–
–	–	601.55	5.103	–	–
$\rho = 271.09\,\mathrm{kg \cdot m^{-3}}$		$\rho = 260.02\,\mathrm{kg \cdot m^{-3}}$		$\rho = 243.98\,\mathrm{kg \cdot m^{-3}}$	
T (K)	C_{VX} $\left(\mathrm{kJ \cdot kg^{-1} \cdot K^{-1}}\right)$	T (K)	C_{VX} $\left(\mathrm{kJ \cdot kg^{-1} \cdot K^{-1}}\right)$	T (K)	C_{VX} $\left(\mathrm{kJ \cdot kg^{-1} \cdot K^{-1}}\right)$
596.64	9.179	600.68	10.50	598.79	10.38
596.73	9.294	600.81	10.46	598.88	10.39
596.86	9.224	600.94	10.55	598.96	10.34
597.03	9.266	601.02	10.65	599.05	10.31
597.16	9.238	601.19	10.59	599.14	10.39
600.77	10.67	601.28	10.66	599.22	10.33
600.85	10.87	601.49	10.60	602.18	10.96
601.02	10.79	601.75	10.65	602.35	11.07
601.24	10.89	601.87	10.72	602.52	11.06
601.37	10.73	601.96	10.78	602.69	11.11
601.45	10.87	602.05	10.74	602.82	10.99
601.24	10.89	602.14	10.84	602.91	10.82
601.37	10.73	602.22	10.87	602.91	5.980

Table 1 continued

$\rho = 271.09\,\mathrm{kg \cdot m^{-3}}$		$\rho = 260.02\,\mathrm{kg \cdot m^{-3}}$		$\rho = 243.98\,\mathrm{kg \cdot m^{-3}}$	
T (K)	C_{VX} $(\mathrm{kJ \cdot kg^{-1} \cdot K^{-1}})$	T (K)	C_{VX} $(\mathrm{kJ \cdot kg^{-1} \cdot K^{-1}})$	T (K)	C_{VX} $(\mathrm{kJ \cdot kg^{-1} \cdot K^{-1}})$
601.45	10.88	602.39	10.86	602.48	5.635
601.58	11.06	602.45	10.73	602.56	5.418
601.75	10.99	602.48	5.635	602.65	5.524
601.91	11.09	602.56	5.418	602.74	5.345
602.05	11.05	602.65	5.524	603.17	5.006
602.05	6.010	602.74	5.345	603.26	4.877
602.08	5.870	603.17	5.006	603.34	4.938
602.09	5.656	603.26	4.877	603.43	4.965
602.12	5.423	603.34	4.938	603.51	4.822
602.24	5.289	603.43	4.965	603.58	4.689
602.38	5.013	603.51	4.822	603.69	4.794
602.51	4.845	603.58	4.689	603.78	4.657
–	–	603.69	4.794	–	–
–	–	603.78	4.657	–	–
–	–	603.86	4.692	–	–
$\rho = 230.31\,\mathrm{kg \cdot m^{-3}}$		$\rho = 227.54\,\mathrm{kg \cdot m^{-3}}$		$\rho = 224.53\,\mathrm{kg \cdot m^{-3}}$	
T (K)	C_{VX} $(\mathrm{kJ \cdot kg^{-1} \cdot K^{-1}})$	T (K)	C_{VX} $(\mathrm{kJ \cdot kg^{-1} \cdot K^{-1}})$	T (K)	C_{VX} $(\mathrm{kJ \cdot kg^{-1} \cdot K^{-1}})$
600.51	10.38	595.74	10.04	598.02	10.53
600.59	10.53	595.78	9.904	598.11	10.59
600.72	10.41	595.91	9.943	598.25	10.55
600.85	10.47	596.04	10.05	598.36	10.49
600.94	10.37	596.09	9.876	598.44	10.52
601.45	10.93	596.21	9.929	601.02	10.72
601.54	11.12	601.28	10.93	601.11	10.84
601.62	11.05	601.37	10.79	601.20	10.81
601.71	11.16	601.45	10.73	601.36	10.93
601.79	11.12	601.57	10.87	601.45	10.81
601.87	11.06	602.65	11.51	601.58	10.89
601.96	11.13	602.74	11.66	601.71	10.92
602.05	11.24	602.82	11.63	602.65	11.06
602.65	11.63	602.91	11.22	602.63	11.17
602.74	11.56	602.97	10.96	602.83	11.09
602.82	11.23	602.97	6.332	602.92	11.02
602.91	11.15	602.99	5.750	602.96	10.86
602.96	10.92	603.08	5.340	602.96	6.252
602.96	6.270	603.16	5.023	602.99	6.170
602.99	5.830	603.25	5.112	603.08	5.750
603.08	5.510	603.59	5.024	603.17	5.569
603.16	5.220	603.68	4.918	603.25	5.368
603.26	5.152	603.76	5.027	603.33	5.344
603.67	4.786	603.85	4.816	603.42	5.361
603.94	4.885	603.93	4.753	603.85	5.293
604.12	4.610	604.02	4.930	603.94	5.344
604.31	4.510	604.11	4.725	604.02	5.171
604.43	4.790	604.19	4.768	604.11	5.306
604.52	4.651	604.28	4.865	604.19	5.251
611.35	4.520	–	–	604.28	5.066

Table 1 continued

$\rho = 230.31\,\mathrm{kg \cdot m^{-3}}$		$\rho = 227.54\,\mathrm{kg \cdot m^{-3}}$		$\rho = 224.53\,\mathrm{kg \cdot m^{-3}}$	
T (K)	C_{VX} $(\mathrm{kJ \cdot kg^{-1} \cdot K^{-1}})$	T (K)	C_{VX} $(\mathrm{kJ \cdot kg^{-1} \cdot K^{-1}})$	T (K)	C_{VX} $(\mathrm{kJ \cdot kg^{-1} \cdot K^{-1}})$
611.44	4.562	–	–	604.36	5.133
611.52	4.369	–	–	604.45	5.115
611.57	4.411	–	–	–	–
611.80	4.340	–	–	–	–
$\rho = 218.92\,\mathrm{kg \cdot m^{-3}}$		$\rho = 214.83\,\mathrm{kg \cdot m^{-3}}$		$\rho = 205.58\,\mathrm{kg \cdot m^{-3}}$	
T (K)	C_{VX} $(\mathrm{kJ \cdot kg^{-1} \cdot K^{-1}})$	T (K)	C_{VX} $(\mathrm{kJ \cdot kg^{-1} \cdot K^{-1}})$	T (K)	C_{VX} $(\mathrm{kJ \cdot kg^{-1} \cdot K^{-1}})$
597.33	10.51	598.79	11.03	599.31	11.01
597.42	10.62	598.88	10.93	599.39	10.93
597.50	10.53	598.96	10.91	599.48	11.14
597.59	10.48	599.05	11.06	599.57	11.00
597.68	10.58	599.19	11.00	599.65	10.93
597.85	10.68	599.31	11.04	599.74	10.92
601.91	11.91	599.39	11.13	599.82	11.05
602.06	12.02	599.48	10.96	601.19	11.10
602.14	11.86	601.10	11.58	601.28	11.03
602.24	11.90	601.30	11.31	601.37	11.02
602.35	11.75	601.28	11.48	601.45	11.17
602.66	11.94	601.37	11.31	601.54	10.90
602.74	11.70	601.45	11.53	601.62	11.12
602.83	11.01	601.54	11.42	601.71	11.02
602.85	10.68	602.40	11.64	601.97	11.39
602.85	6.110	602.47	11.68	602.05	11.18
602.91	5.580	602.56	11.53	602.14	11.15
603.01	5.234	602.67	11.31	602.22	10.99
603.08	5.263	602.74	10.45	602.24	10.54
603.77	5.060	602.74	6.020	602.26	10.21
603.86	4.894	602.82	5.785	602.26	5.930
–	–	602.91	5.309	602.31	5.660
–	–	602.99	5.143	602.39	4.880
–	–	603.08	5.176	602.48	4.250
–	–	603.10	4.805	602.56	4.340
–	–	603.60	4.824	602.74	4.163
–	–	603.68	4.762	603.08	4.013
–	–	603.77	4.607	603.16	3.995
–	–	603.92	4.762	603.25	4.140
–	–	604.04	4.553	603.34	3.924
–	–	604.09	4.649	603.42	3.822
–	–	604.20	4.623	603.51	4.065
–	–	604.28	4.477	603.59	3.886
$\rho = 195.99\,\mathrm{kg \cdot m^{-3}}$		$\rho = 188.05\,\mathrm{kg \cdot m^{-3}}$		$\rho = 160.07\,\mathrm{kg \cdot m^{-3}}$	
T (K)	C_{VX} $(\mathrm{kJ \cdot kg^{-1} \cdot K^{-1}})$	T (K)	C_{VX} $(\mathrm{kJ \cdot kg^{-1} \cdot K^{-1}})$	T (K)	C_{VX} $(\mathrm{kJ \cdot kg^{-1} \cdot K^{-1}})$
599.99	11.39	592.44	9.371	583.61	8.876
600.08	11.38	592.53	9.329	583.69	8.813
600.17	11.48	592.58	9.230	583.77	8.722

Table 1 continued

$\rho = 195.99\,\mathrm{kg \cdot m^{-3}}$		$\rho = 188.05\,\mathrm{kg \cdot m^{-3}}$		$\rho = 160.07\,\mathrm{kg \cdot m^{-3}}$	
T (K)	C_{VX} $\left(\mathrm{kJ \cdot kg^{-1} \cdot K^{-1}}\right)$	T (K)	C_{VX} $\left(\mathrm{kJ \cdot kg^{-1} \cdot K^{-1}}\right)$	T (K)	C_{VX} $\left(\mathrm{kJ \cdot kg^{-1} \cdot K^{-1}}\right)$
600.25	11.44	592.70	9.260	583.99	8.915
600.34	11.28	592.76	9.270	591.03	9.670
600.42	11.24	592.86	9.432	591.13	9.721
600.51	11.30	592.93	9.508	591.23	9.781
601.45	11.33	597.09	10.39	591.31	9.825
601.54	11.22	597.17	10.49	591.39	9.756
601.62	10.57	597.26	10.53	591.49	9.839
601.71	10.16	597.34	10.55	591.59	9.817
601.75	9.320	597.43	10.44	595.60	10.10
601.75	5.850	597.49	10.52	595.68	10.16
601.79	5.338	597.58	10.41	595.80	10.14
601.89	4.933	600.48	10.55	595.86	10.19
601.98	4.382	600.75	10.25	595.97	10.05
602.62	4.104	600.86	10.43	596.02	10.11
606.33	3.502	600.92	9.930	596.80	10.11
606.41	3.502	601.03	9.740	596.99	10.16
606.50	3.516	601.11	9.390	597.16	9.966
606.66	3.492	601.16	9.108	597.48	9.370
606.75	3.509	601.16	5.978	597.35	8.834
606.84	3.498	601.20	5.290	597.35	5.743
609.06	3.499	601.30	4.870	597.38	4.600
609.14	3.531	601.38	3.757	597.43	3.912
609.23	3.507	601.50	4.060	597.53	3.526
609.30	3.565	601.56	3.466	597.60	3.765
609.40	3.528	601.75	3.649	597.69	3.688
609.48	3.558	–	–	598.98	3.281
609.74	3.509	–	–	599.12	3.203
–	–	–	–	599.24	3.352
–	–	–	–	599.28	3.234
–	–	–	–	608.19	2.980
–	–	–	–	608.40	3.016
–	–	–	–	608.54	2.914
–	–	–	–	608.63	3.007
–	–	–	–	608.72	2.934
–	–	–	–	608.81	2.955
–	–	–	–	608.90	2.948
–	–	–	–	615.18	3.220
–	–	–	–	615.27	3.230
–	–	–	–	615.35	3.332
–	–	–	–	615.52	3.253
–	–	–	–	615.61	3.218
–	–	–	–	615.69	3.284
–	–	–	–	615.78	3.368
–	–	–	–	624.74	3.472
–	–	–	–	624.83	3.575
–	–	–	–	624.99	3.547
–	–	–	–	625.08	3.432
–	–	–	–	625.16	3.618
–	–	–	–	633.07	3.809
–	–	–	–	633.16	3.869

Table 1 continued

$\rho = 195.99\,\mathrm{kg \cdot m^{-3}}$		$\rho = 188.05\,\mathrm{kg \cdot m^{-3}}$		$\rho = 160.07\,\mathrm{kg \cdot m^{-3}}$	
T (K)	C_{VX} $\left(\mathrm{kJ \cdot kg^{-1} \cdot K^{-1}}\right)$	T (K)	C_{VX} $\left(\mathrm{kJ \cdot kg^{-1} \cdot K^{-1}}\right)$	T (K)	C_{VX} $\left(\mathrm{kJ \cdot kg^{-1} \cdot K^{-1}}\right)$
–	–	–	–	633.33	3.783
–	–	–	–	633.49	3.857
–	–	–	–	633.58	3.796
–	–	–	–	633.66	3.828

$\rho = 147.43\,\mathrm{kg \cdot m^{-3}}$		$\rho = 120.03\,\mathrm{kg \cdot m^{-3}}$	
T (K)	$C_{VX}\left(\mathrm{kJ \cdot kg^{-1} \cdot K^{-1}}\right)$	T (K)	$C_{VX}\left(\mathrm{kJ \cdot kg^{-1} \cdot K^{-1}}\right)$
576.71	7.958	575.66	8.230
576.62	7.757	575.75	8.563
576.54	7.856	575.84	8.389
576.45	7.903	581.68	9.260
585.68	8.991	581.77	9.070
585.59	8.969	581.86	9.130
585.50	8.809	581.94	9.010
585.42	8.681	582.03	9.144
585.33	8.727	582.29	9.086
592.29	9.842	584.44	9.710
592.49	9.966	584.52	9.750
592.68	9.835	584.90	9.781
592.89	9.914	584.98	9.775
593.11	9.924	585.07	9.647
593.29	9.882	585.16	9.622
593.37	9.766	585.31	9.456
593.46	9.605	585.31	6.500
593.72	9.633	585.34	6.208
593.80	9.433	585.40	5.460
593.89	9.503	585.48	5.342
593.98	9.359	585.62	4.332
594.06	9.145	585.94	3.620
594.14	8.932	586.02	3.352
594.14	5.852	586.11	3.273
594.15	5.239	586.20	3.040
594.23	5.137	586.28	3.070
594.32	4.652	586.37	2.880
594.49	4.529	595.01	2.690
594.58	3.790	594.78	2.659
594.66	3.505	594.75	2.610
594.75	3.425	594.66	2.640
594.84	3.236	594.58	2.450
594.92	3.007	–	–
595.09	3.194	–	–
595.18	2.964	–	–
595.44	2.817	–	–
595.70	2.971	–	–
605.39	3.110	–	–
605.47	2.960	–	–
605.64	3.083	–	–
605.73	3.101	–	–
605.82	3.143	–	–
605.90	3.068	–	–

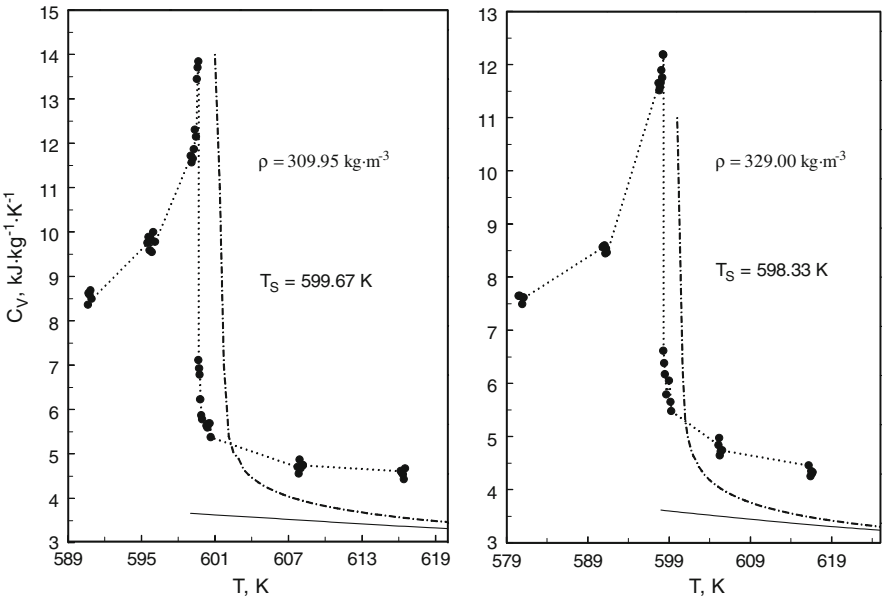

Fig. 1 Measured single- and two-phase isochoric heat capacities of 0.2607 $NH_3 + 0.7393\,H_2O$ along the two selected near-critical isochores as a function of temperature near the phase transition points together with the values calculated from EOS, (—) Friend and Tillner-Roth [28] EOS, (–·–·–·–) crossover model by Kiselev and Rainwater [29], (. . ..) connecting the experimental data or experimental curve

3.1 Liquid and Vapor Single- and Two-Phase Isochoric Heat Capacity at Saturation and in the Retrograde Region

Table 2 shows the values of the phase boundary properties (T_S, ρ'_S, ρ''_S, C'_{V1}, C'_{V2}, C''_{V1}, C''_{V2}) derived with the quasi-static thermogram technique. In Figs. 6, 7, 8, the temperature and specific volume dependences of the measured values of (C'_{V1}, C'_{V2}, C''_{V1}, C''_{V2}) along the saturation curve are presented. A detailed view of the single-phase liquid (C'_{V1}) and single-phase vapor (C''_{V1}) isochoric heat-capacity behavior at saturation in the region near the critical and maxcondentherm points is shown in Figs. 7 and 8. As one can see from Fig. 7 (right), the single-phase vapor isochoric heat capacity C''_{V1} is split into two branches. One of them originates from the maxcondentherm temperature $T_m = 602.97$ K and goes through a temperature minimum at approximately 602.3 K and terminates at the critical point $T_C = 599.67$ K (connecting with the one-phase liquid isochoric heat capacity C'_{V1}). Thus, the vapor branch of the single-phase curve, C''_{V1}–T, intersects with the liquid branch of the single-phase curve, C'_{V1}–T at the critical point, i.e., liquid C'_{V1}–T curve cuts the vapor C''_{V1}–T branch of the saturated curve at the critical point where liquid and vapor phases become identical.

The second branch of the single-phase vapor isochoric heat-capacity curve (C''_{V1}–T) commences from the maxcondentherm point and passes through a temperature minimum at approximately 598 K. For an ordinary mixture (without retrograde phenomena), the temperatures $T_m = T_C$ and the behavior of the isochoric heat capacity near the critical point are as usual; there is no first branch of the single-

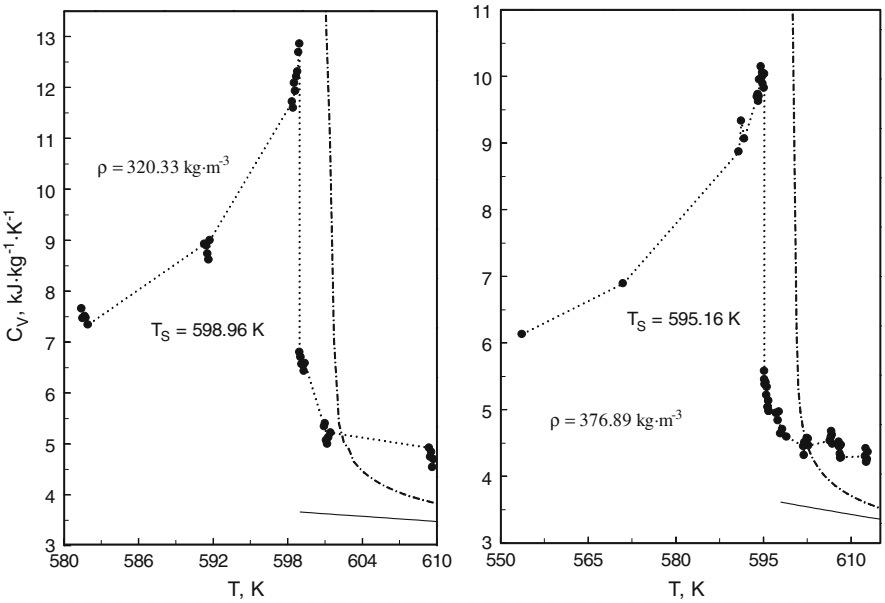

Fig. 2 Measured single- and two-phase isochoric heat capacities of 0.2607 $NH_3 + 0.7393\,H_2O$ along the two selected near-critical isochores as a function of temperature near the phase transition points together with the values calculated from EOS, (—) Friend and Tillner-Roth [28] EOS, (–·–·–·–) crossover model by Kiselev and Rainwater [29], (. . ..) connecting the experimental data or experimental curve

phase vapor isochoric heat-capacity curve (C''_{V1}–T). The width of the retrograde range (the difference between T_m and T_C points) varies depending on the nature of the pure component interactions. The liquid single-phase isochoric heat capacity at saturation behavior, C'_{V1}–T, as is usual for binary mixtures, proceeds directly to the critical point without passing through a temperature minimum and connects with the first branch of the C''_{V1}–T curve. The first branch of the C''_{V1}–T curves corresponds to the CPDB part of the P–T diagram, and the second branch corresponds to the BA part of the P–T diagram (see Fig. 9). The single-phase liquid curve at saturation C'_{V1}–T corresponds to the ECP part of the P–T diagram (see Fig. 9). Figure 7 (left) demonstrates the two-phase liquid and vapor isochoric heat-capacity behavior of the mixture near the critical and maxcondentherm points. The two-phase liquid isochoric heat capacity C'_{V2} behaves just like an ordinary binary mixture, while the two-phase vapor isochoric heat capacity passes through a temperature maximum at the maxcondentherm temperature $T_m = 602.97$ K and terminates at the critical temperature, $T_C = 599.67$ K. The two-phase liquid curve, C'_{V2}–T, corresponds to the CPDBA part of the P–T diagram (see Fig. 9). Thus, when compressing the system along the isotherms between T_m and T_C (see Fig. 9), the system crosses the vapor branch of the saturation curve twice. The transition, vapor to vapor–liquid to vapor, occurs (first kind of isothermal retrograde phenomena, see Fig. 9).

The isochoric heat-capacity behavior of the mixture along the selected isotherm $T = 601$ K between the critical and maxcondentherm temperatures ($T_C < T <$

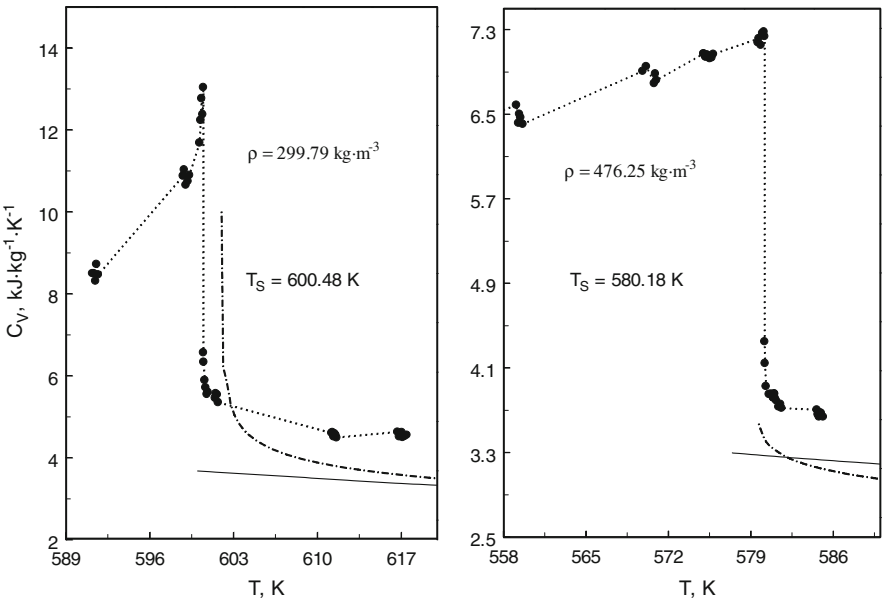

Fig. 3 Measured single- and two-phase isochoric heat capacities of 0.2607 $NH_3 + 0.7393\,H_2O$ along the two selected isochores as a function of temperature near the phase transition points together with the values calculated from EOS, (—) Friend and Tillner-Roth [28] EOS, (–·–·–·–) crossover model by Kiselev and Rainwater [29], (. . ..) connecting the experimental data or experimental curve

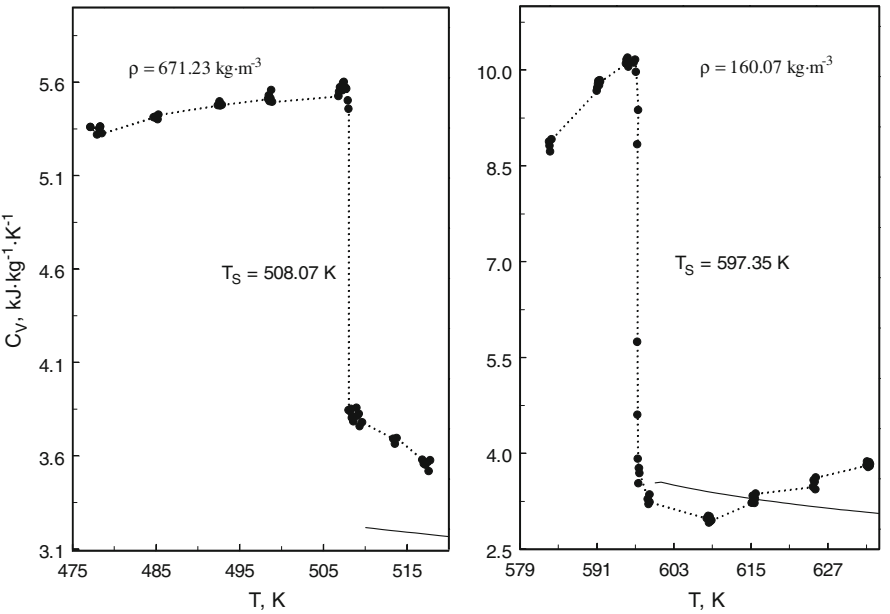

Fig. 4 Measured single- and two-phase isochoric heat capacities of 0.2607 $NH_3 + 0.7393\,H_2O$ along the two selected liquid and vapor isochores as a function of temperature near the phase transition points together with the values calculated from EOS, (—) Friend and Tillner-Roth [28] EOS, (. . ..) connecting the experimental data or experimental curve

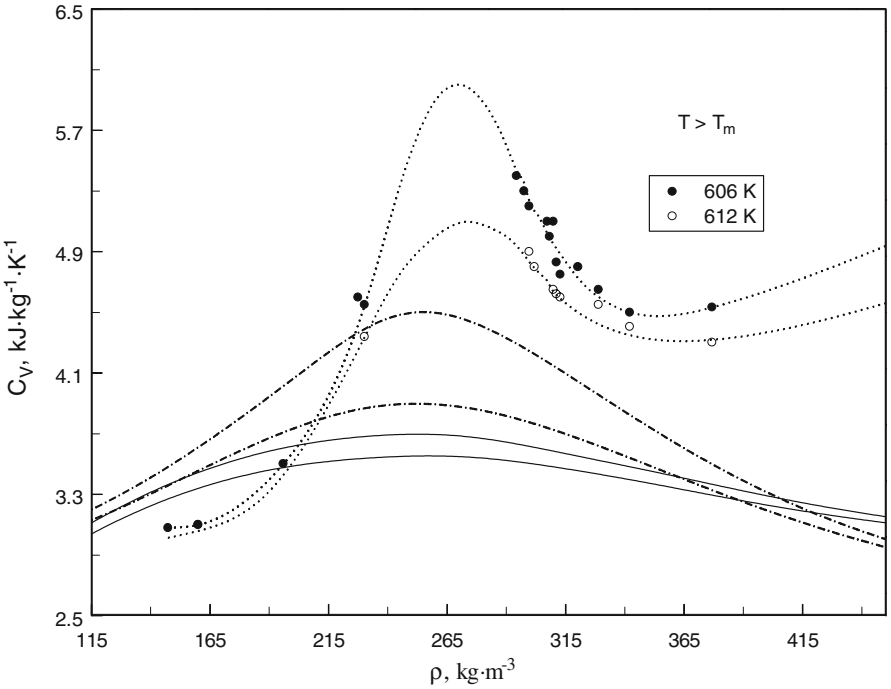

Fig. 5 Measured values of the isochoric heat capacity of 0.2607 NH_3 + 0.7393 H_2O along the two selected supercritical isotherms as a function of density together with the values calculated from EOS, (—) Tillner-Roth and Friend [28], (–·–·–·–) Kiselev and Rainwater [29], (. . .) guide the eye or smoothed curves

T_m) is presented in Fig. 10. As one can see from Fig. 10, isothermal compression of the mixture leads to phase transitions at densities of $\rho''_{1S} = 188.0\,\mathrm{kg \cdot m^{-3}}$ and $\rho''_{2S} = 292.95\,\mathrm{kg \cdot m^{-3}}$. A transition, vapor ⇒ liquid–vapor ⇒ vapor, occurs with an increase and decrease in the heat capacity. The jumps in a C_V–ρ plot mean that the number of phases in the system has changed, increasing or decreasing, depending on increasing or decreasing C_V, after the phase transition point. The first jump at $\rho''_{1S} = 188.0\,\mathrm{kg \cdot m^{-3}}$ corresponds to the intersection of the dew curve (point A in Fig. 9), where the heat capacity increases discontinuously with increasing heat capacity. The vapor phase begins to condense (first appearance of liquid phase is observed) and the number of phases in the system increases, a transition takes place from one vapor to two vapor–liquid phases, vapor ⇒ liquid–vapor. On further compression of the mixture, the liquid-phase volume increases slowly until a maximum is reached (point B in Fig. 9).

The heat capacity is almost linearly increasing, just like the two-phase C_V for pure fluids. At the second phase transition point, $\rho''_{2S} = 292.95\,\mathrm{kg \cdot m^{-3}}$, C_V drops discontinuously. This means that the number of phases in the system decreases, and the liquid volume decreases rapidly and completely disappears at point D. A transition takes place from two vapor–liquid regions to one vapor (disappearance of liquid phase is observed, the liquid phase is vaporized). The range between the jumps (AD, Fig. 9) is the retrograde region. The isochoric heat capacity in the retrograde range is just like the two liquid–gas phase C_V behavior for pure fluids. Figure 8 demonstrates the

Table 2 Isochoric heat capacities of $NH_3 + H_2O$ mixture at saturation ($x = 0.2607$ mole fraction of NH_3)

T_S (K)	ρ_S ($kg \cdot m^{-3}$)	C_{V2} ($kJ \cdot kg^{-1} \cdot K^{-1}$)	C_{V1} ($kJ \cdot kg^{-1} \cdot K^{-1}$)
508.07	671.23	5.456	3.843
519.77	649.65	5.607	3.875
545.62	594.32	5.971	4.015
561.03	552.58	6.367	4.122
565.36	540.25	6.450	4.140
580.18	476.26	7.237	4.350
584.95	456.58	7.760	4.620
595.16	376.89	10.04	5.580
597.56	342.19	11.19	6.250
598.33	329.00	12.18	6.610
598.96	320.33	12.86	6.802
599.42	312.91	13.25	6.990
599.57	311.19	13.55	7.060
599.67[a]	309.95	13.84	7.110
599.78	308.35	13.71	6.990
599.89	307.35	13.51	6.820
600.02	305.44	13.38	6.730
600.17	303.47	13.24	6.680
600.29	301.94	13.15	6.620
600.48	299.79	13.04	6.570
600.63	297.60	12.78	6.470
600.81	295.31	12.64	6.410
600.93	292.97	12.35	6.310
601.05	291.16	12.03	6.270
601.34	285.71	11.51	6.080
602.05	271.09	11.05	6.010
602.45	260.02	10.73	5.920
602.91	243.98	10.82	5.980
602.96	230.31	10.92	6.270
602.97[b]	227.54	10.96	6.332
602.96	224.53	10.86	6.252
602.85	218.92	10.68	6.110
602.74	214.83	10.45	6.020
602.26	206.00	9.810	5.930
601.75	195.99	9.320	5.850
601.16	188.05	9.108	5.778
597.36	160.07	8.834	5.743
594.14	147.43	8.932	5.852
585.31	120.03	9.456	6.500

[a] Critical point
[b] Maxcondentherm point

specific volume dependence of the single- and two-phase isochoric heat capacities of the mixture along the saturation curve. As we can note, two maxima of the C_{V1}–V and C_{V2}–V are exhibited at the critical and maxcondentherm points.

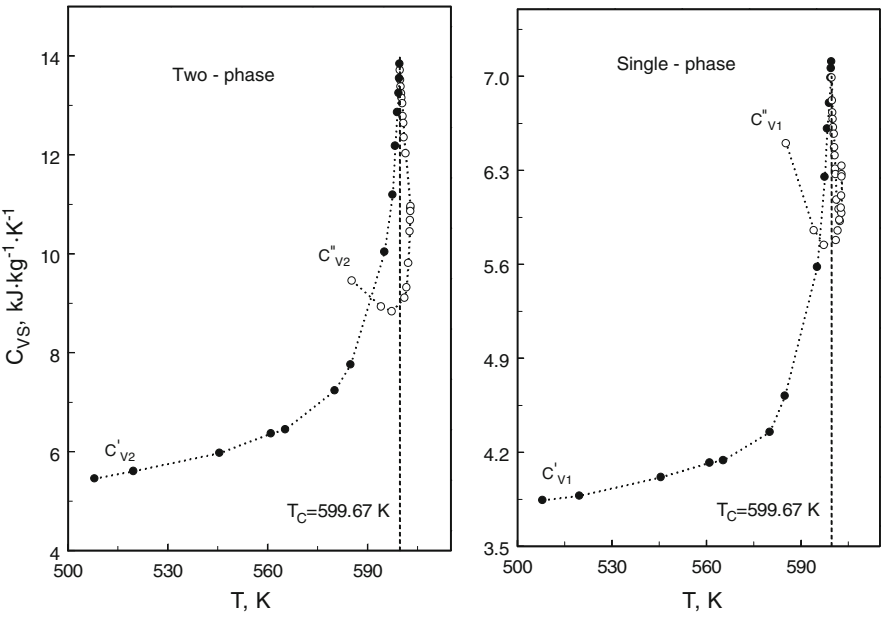

Fig. 6 Measured values of single- (*right*) and two-phase (*left*) liquid and vapor isochoric heat capacity of 0.2607 NH_3 + 0.7393 H_2O along the coexistence curve as a function of temperature

3.2 Liquid- and Vapor-Saturated Densities

The measured saturation liquid and vapor densities for the 0.2603 NH_3 + 0.7397 H_2O mixture are presented in Table 2 and shown in Fig. 11 together with the data reported by other authors and calculated with EOS by Tillner-Roth and Friend [28] and cross-over model by Kiselev and Rainwater [29]. An expanded view (shape) of the measured saturated densities near the critical and maxcondentherm points is shown in Fig. 12. As one can see, the critical point does not coincide with the maximum temperature or the maxcondetherm point as they do for a pure fluid. The coexistence curve has two points of inflection which bracket the critical point. The width of the retrograde range is approximately $T_m - T_C = 3.3$ K. For some other mixtures, the width of the retrograde range is large. The measured values of the saturated density agree with the values calculated from the Tillner-Roth and Friend [28] EOS within 0.4 % for saturated liquid densities, 1.0 % to 3 % in the critical region, and 3 % to 5.5 % for saturated vapor densities.

3.3 Critical Parameters

Figures 7 and 8 illustrate the temperature and specific volume dependences of the single- and two-phase liquid (C'_{V2}, C'_{V1}) and vapor (C''_{V2}, C''_{V1}) isochoric heat capacities of the 0.2603 NH_3 + 0.7397 H_2O mixture at saturation near the critical

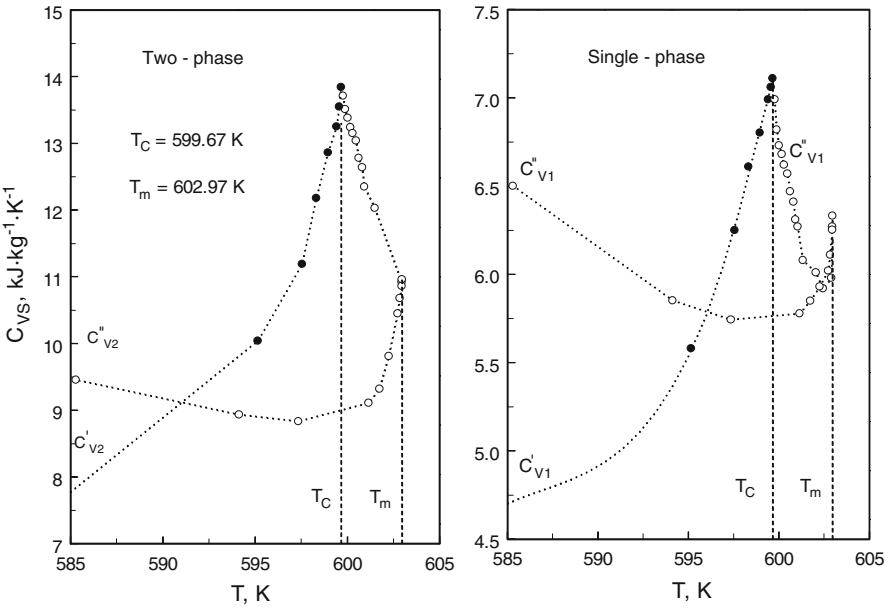

Fig. 7 Expanded view of the measured values of single- and two-phase (liquid and vapor) isochoric heat capacity of 0.2607 NH_3 + 0.7393 H_2O along the coexistence curve near the critical (T_c) and maxcondentherm (T_m) points

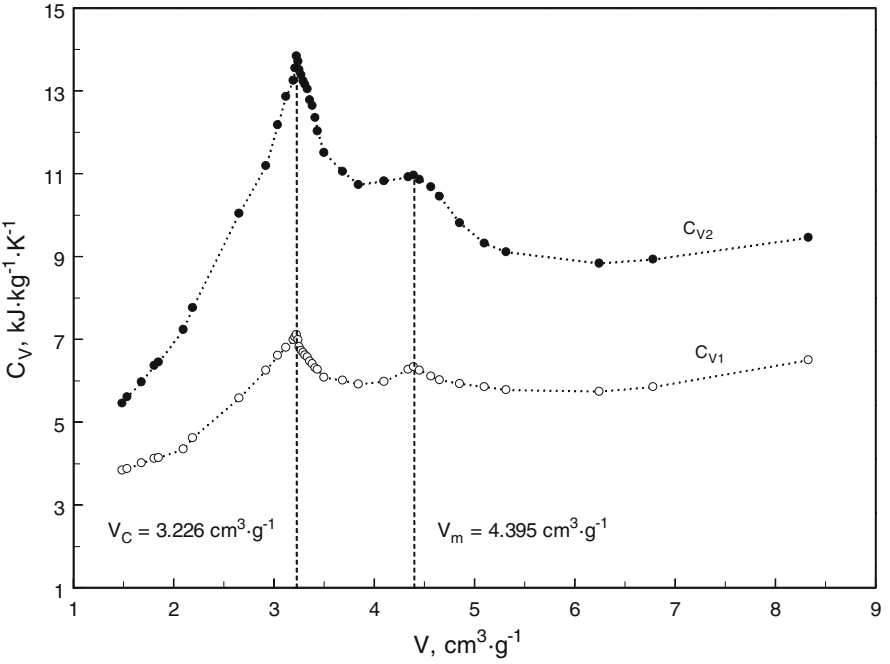

Fig. 8 Measured single- and two-phase isochoric heat capacities of 0.2607 NH_3 + 0.7393 H_2O along the coexistence curve as a function of specific volume near the critical (V_C) and maxcondentherm (V_m) points

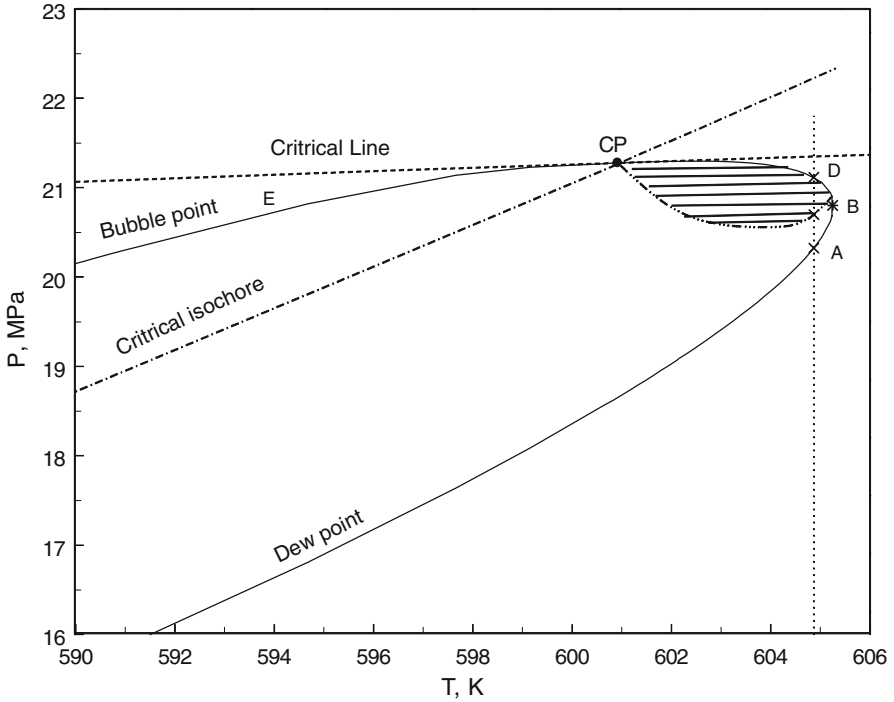

Fig. 9 Pressure–temperature diagram of $NH_3 + H_2O$ mixture near the critical and maxcondentherm points (first kind retrograde phenomena) calculated from Tillner-Roth and Friend [28] EOS

and maxcondentherm points. As one can see from Figs. 7 and 8, the single- and two-phase liquid and vapor branches of the saturated isochoric heat capacities coincide (both liquid and vapor phases become identical) at the critical point of (599.67 ± 0.2) K, providing the temperature of the critical point of the mixture. On the saturated density curve (Fig. 12), this critical temperature corresponds to a critical density of $(310.95 \pm 0.5)\ \mathrm{kg \cdot m^{-3}}$. The critical temperature and density obtained are in reasonable agreement with the data reported by other authors (see Figs. 13 and 14). Our value of $T_C = (599.67 \pm 0.2)$ K is in satisfactory (difference within 0.97 K and 1.42 K) agreement with the interpolated values calculated from the data by Sassen et al. [47] and Tsiklis et al. [48], but is significantly lower (by 6.97 K) than the value reported by Rizvi and Heidemann [46]. It is in satisfactory agreement within 1.23 K (our result lower) with the values calculated using crossover models by Kiselev and Rainwater [29], and Rainwater and Tillner-Roth [30]. The value of the critical density predicted with the crossover models [29,30] ($323.11\ \mathrm{kg \cdot m^{-3}}$) agrees with the present result within 3.9 %. Our result for the critical density also satisfactorily (difference is 3.7 %) agrees with the value calculated with the Tillner-Roth and Friend [28] EOS.

The present results for the critical parameters of the 0.2603 NH_3 + 0.7397 H_2O mixture together with the reported data are presented in Figs. 13 and 14 in various projections. As one can see from Figs. 13 and 14, T_C–x, P_C–x, P_C–T_C, and ρ_C–T_C curves show slightly positive deviations from the ideal mixture behavior. The slope,

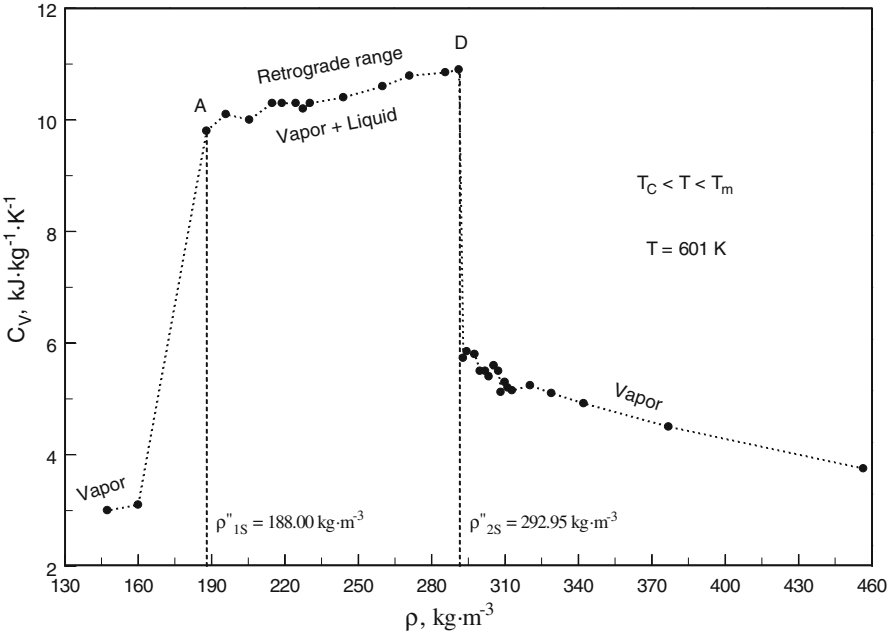

Fig. 10 Measured values of isochoric heat capacity of 0.2607 NH_3 + 0.7393 H_2O along the selected isotherm between critical and maxcondentherm temperatures in the retrograde range as a function of density (vapor ⇒ vapor + liquid ⇒ vapor transition)

$(dP_C/dT_C)^C_{CRL}$, of the P_C–T_C projection of the critical locus at the pure water critical point is positive and lower than the slope of the vapor-pressure curve, $(dP_S/dT)^C_{CXC}$, of pure water at its critical point. As will be shown below, this is very important to calculate the value of the Krichevskii parameter and thermodynamic properties of dilute $NH_3 + H_2O$ mixtures near the critical point of pure water.

The present critical property data for the 0.2603 NH_3 + 0.7397 H_2O mixture together with published data were fitted to an empirical polynomial function as a function of composition

$$T_C(x) = (1-x)T_{C1} + xT_{C2} + x(1-x)\left[T_1 + (1-2x)T_2 + (1-2x)^2 T_3\right], \quad (3)$$

$$P_C(x) = (1-x)P_{C1} + xP_{C2} + x(1-x)\left[P_1 + (1-2x)P_2 + (1-2x)^2 P_3\right], \quad (4)$$

where $T_{C1} = 647.096$ K, $P_{C1} = 22.064$ MPa (pure water, IAPWS [70] accepted values), $T_{C2} = 405.4$ K, and $P_{C1} = 11.333$ MPa (pure ammonia [76,77]). The derived values of fitting parameters (T_i and P_i, $i = 1, 3$) are as follows: $T_1 = 91.60579$; $T_2 = -33.65308$; $T_3 = -3.45447$; $P_1 = 13.77987$; $P_2 = -8.06646$; and $P_3 = 2.96368$. These values were used to calculate the Krichevskii parameter (see Sect. 3.3) and characteristic parameters, K_1, K_2, τ_1, τ_2, $\Delta\rho_1$, and $\Delta\rho_2$ (see Sect. 4.2) for the 0.2603 NH_3 + 0.7397 H_2O mixture.

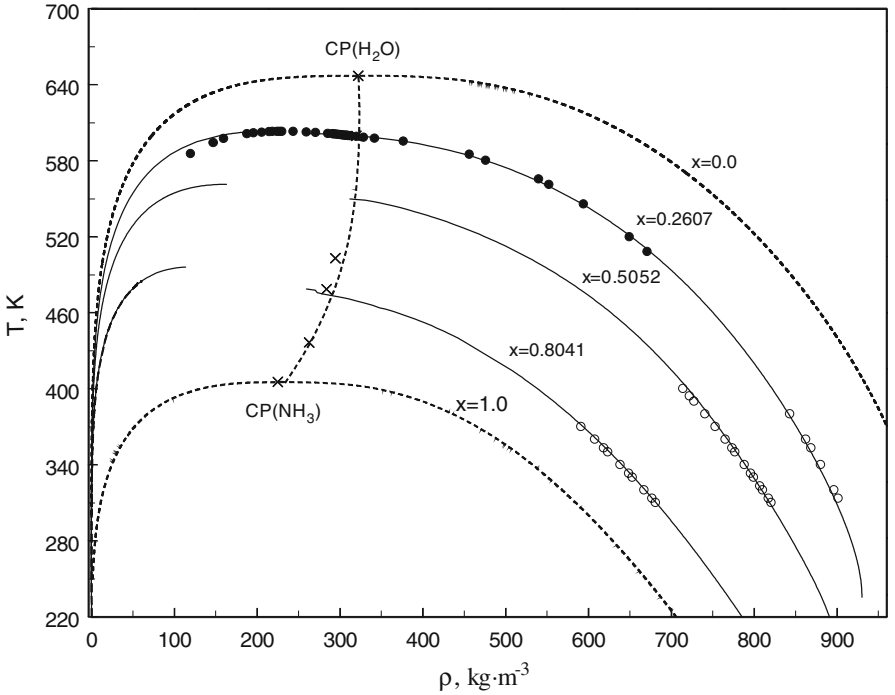

Fig. 11 Measured saturated liquid and vapor densities of $NH_3 + H_2O$ mixtures together with the values reported by other authors and calculated from EOS, (—) Friend and Tillner-Roth [28], (– – –) coexistence curves for pure components calculated from EOS [70,77]; •—this study, ○—Suzuki and Uematsu [42]

4 Krichevskii Parameter: Thermodynamic and Structural Properties of Dilute $NH_3 + H_2O$ Mixture near the Critical Point of Pure Water

4.1 Shape of the Critical Lines and Krichevskii Parameter

The Krichevskii parameter plays a very important role in near-critical solution thermodynamics [78–83], particularly in determining the thermodynamic behavior of dilute solutions near the solvent's critical point. In general, the thermodynamic behavior of infinitely dilute mixtures near the solvent's critical point can be completely characterized by the Krichevskii parameter which is equal to the derivative $(\partial P/\partial x)^{\infty}_{T_C V_C}$ calculated at the critical point of the pure solvent. Using the concept of the Krichevskii parameter, Levelt-Sengers [78–81] proposed a description of thermodynamic behavior of dilute near-critical solutions based on the derivative $(\partial P/\partial x)^{\infty}_{TV}$ (Krichevskii function J [84,85]). The Krichevskii parameter governs the thermodynamic properties of a dilute solute in the vicinity of the critical point of a pure solvent. For example, in the limit of infinite dilution, many partial molar properties of the solute ($\bar{V}_2^{\infty}$, $\bar{H}_2^{\infty}$, $\bar{C}_{p2}^{\infty}$), which are related to the Krichevskii parameter, are strongly divergent at the solvent's critical point [86–94]. The vapor–liquid distribution coefficient $K_D$of the solute at infinite dilution between vapor and liquid solvents, $RT \ln K_D \approx$

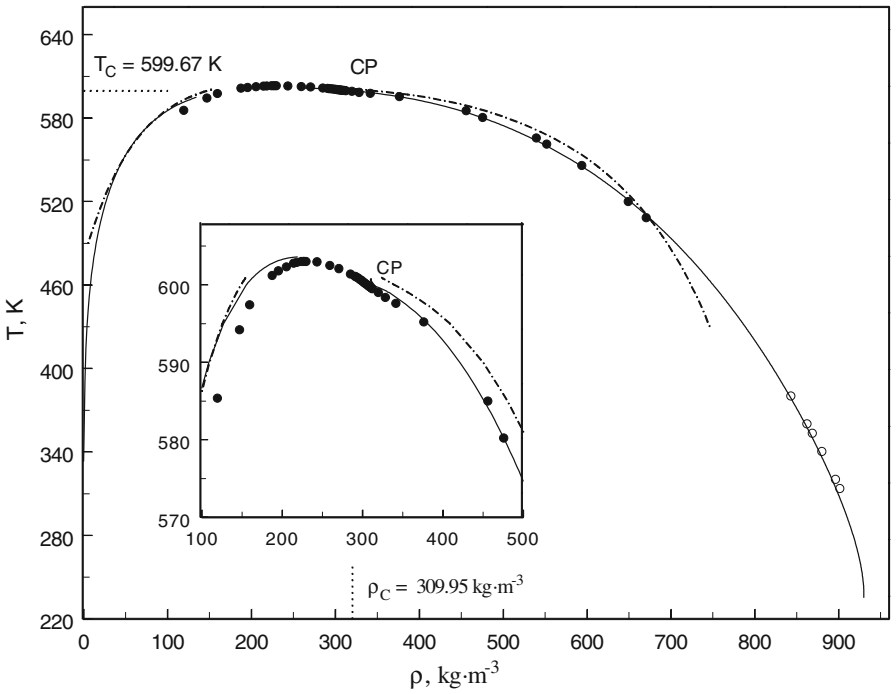

Fig. 12 Measured saturated liquid and vapor densities of 0.2607 NH_3 + 0.7393 H_2O together with the values reported by other authors and calculated from EOS in the critical and retrograde regions (—) Friend and Tillner-Roth [28], (–·–·–·–) crossover model (Kiselev and Rainwater [29]); •—this study, ○—Suzuki and Uematsu [42]

$-\left(2J/\rho_{C1}^2\right)[\rho(1)-\rho_{C1}]$, is also directly related to the Krichevskii function, $J = (\partial P/\partial x)_{TV}^{\infty}$, [78–95]. The limiting slope of $RT \ln K_D$ as a function of the liquid-phase density $[\rho(1)-\rho_{C1}]$, as the system approaches the critical point, is also given by the Krichevskii parameter as $-2\,(\partial P/\partial x)_{T_C V_C}^{\infty}/\rho_{C1}^2$, Henry's constant K_H near the critical point [95,96], $(T \ln (K_H/f_1)$, and $T \ln E$ (where $E = y_2 P/P_2^{sub}$ is the enhancement factor; P, y_2, P_2^{sub} are the pressure, solubility, and sublimation pressure, respectively) are linear in the solvent density, with the slope given by the Krichevskii parameter. The Krichevskii parameter also determines the shape of the dew-bubble curves, isothermal in $P-x$ space and isobaric in $T-x$ space [78–80].

The Krichevskii function, $J = (\partial P/\partial x)_{TV}^{\infty}$, has a simple physical means and a straight-forward connection to total and direct correlation function integrals (TCFI and DCFI) [96–102] and takes into account the effects of the intermolecular interactions between solvent and solute molecules that determine the thermodynamic properties of dilute solutions. The values of $(\partial P/\partial x)_{TV}^{\infty}$ are related also to the behavior of the microstructure parameters of dilute supercritical solutions (cluster size, N_{clus}), see Sect. 4.3.

The Krichevskii parameter can be estimated from the initial slopes, (dT_C/dx) and (dP_C/dx), of the $T_C(x)$and $P_C(x)$ critical lines of the mixture and the value of the vapor–pressure curve slope $(dP_S/dT)_{CXC}^{C}$of pure water (pure solvent) at the critical

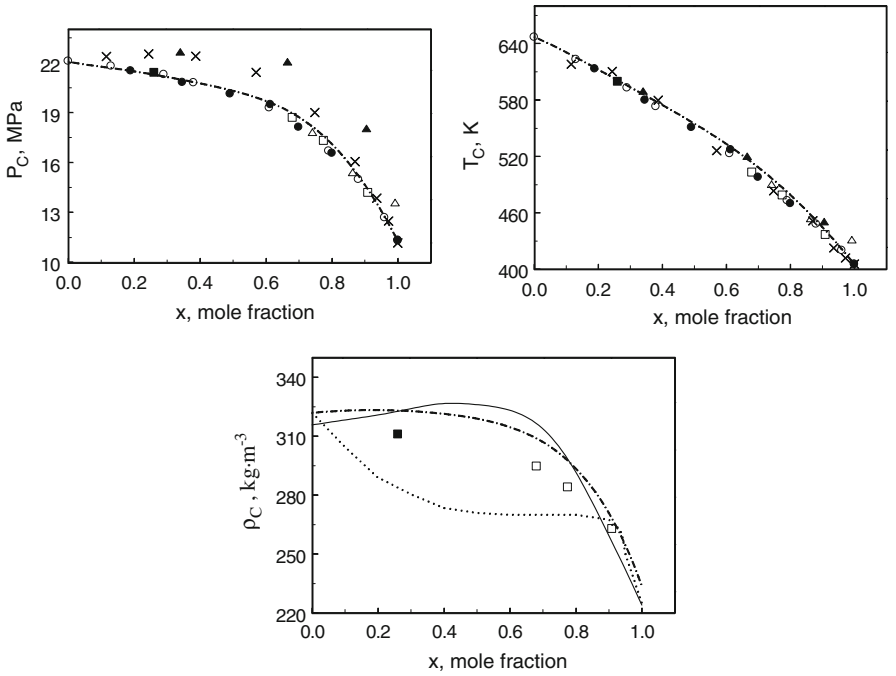

Fig. 13 Critical properties of $NH_3 + H_2O$ mixture reported by various authors in the P_C–x, T_C–x, and ρ_C–x projections; •—Sassen et al. [47], ○—Tsiklis et al. [48], ■—this study, □—Sakabe et al. [50], ×—Rizvi and Heidemann [46], △—Postma [49], ▲—Gillespie et al. [51]; (—) Tillner–Roth and Friend [28], (–·–·–·–) crossover model (Kiselev and Rainwater [29]), (· · · · ·) Suzuki and Uematsu [42]

point. Krichevskii [103] derived the relation between the initial slopes of the critical lines and the derivative $(\partial P/\partial x)^{\infty}_{T_C V_C}$,

$$\left(\frac{\partial P}{\partial x}\right)^{\infty}_{V_C T_C} = \left(\frac{\mathrm{d}P_C}{\mathrm{d}x}\right)^{C}_{CRL} - \left(\frac{\mathrm{d}P_S}{\mathrm{d}T}\right)^{C}_{CXC}\left(\frac{\mathrm{d}T_C}{\mathrm{d}x}\right)^{C}_{CRL}, \tag{5}$$

or in equivalent form,

$$\left(\frac{\partial P}{\partial x}\right)^{C}_{V_C T_C} = \left[\left(\frac{\mathrm{d}P_C}{\mathrm{d}T_C}\right)^{C}_{CRL} - \left(\frac{\mathrm{d}P_S}{\mathrm{d}T}\right)^{C}_{CXC}\right]\left(\frac{\mathrm{d}T_C}{\mathrm{d}x}\right)^{C}_{CRL}, \tag{6}$$

where "CXC" and "CRL" subscripts are related to the vapor-pressure and critical line curves, respectively. The regimes of the near-critical dilute solution behavior depend strongly on the signs and magnitudes of the initial slopes of the critical curves $T_C(x)$, $P_C(x)$, and on the slope of the vapor–pressure curve $(\mathrm{d}P_S/\mathrm{d}T)^{C}_{CXC}$ at the critical point of the pure solvent, i.e., the magnitude and sign of the Krichevskii parameter, $(\partial P/\partial x)^{C}_{T_C V_C}$. The value of the derivative $(\mathrm{d}P_S/\mathrm{d}T)^{C}_{CXC} = 0.2682\,\mathrm{MPa}\cdot\mathrm{K}^{-1}$ for pure water is calculated with the vapor–pressure equation (IAPWS formulation, Levelt-Sengers [104]), and the slopes of the critical lines $T_C(x)$ and $P_C(x)$ from Eqs.

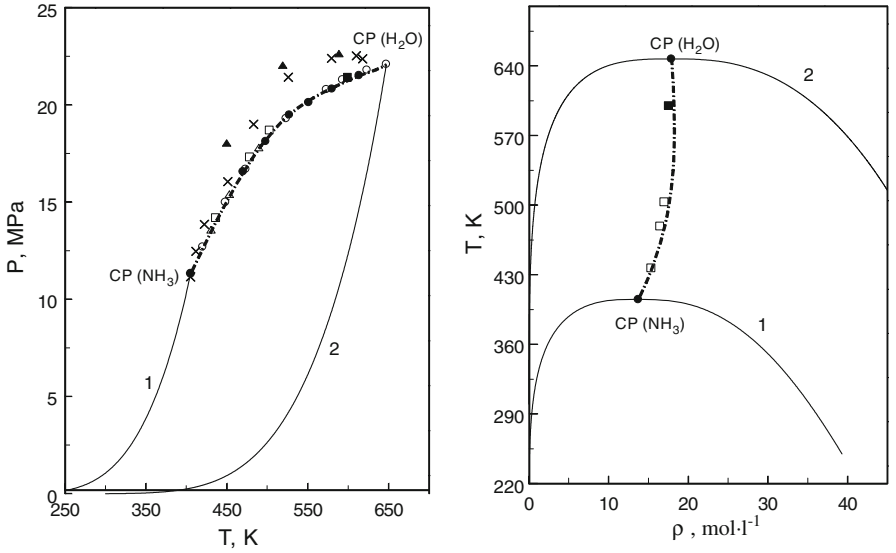

Fig. 14 Critical properties of $NH_3 + H_2O$ mixture reported by various authors in the P_C–T_C and T_C–ρ_C projections; 1 and 2 are the vapor pressure and coexistence curves of ammonia [75,76] and water (IAPWS [69]), respectively; •—Sassen et al. [47], ○—Tsiklis et al. [48], ■—this study, □—Sakabe et al. [50], ×—Rizvi and Heidemann [46], △— Postma [49], ▲—Gillespie et al. [51]; (–·–·–·–) crossover model (Kiselev and Rainwater [29]), (—) were calculated from EOS for pure components [70,77]

3 and 4. The value of $(\partial P_C/\partial T_C)_{CRL}$ for $NH_3 + H_2O$ at the critical point of pure water is lower than the value of the vapor–pressure curve $(dP_S/dT)^C_{CXC}$ for water at the critical point (see Fig. 14). Therefore, as one can see from Eq. 6, the value of the Krichevskii parameter of $NH_3 + H_2O$ is positive (the value of the derivative $(dT_C/dx)_{CRL} < 0$ is negative). The values of the derivatives $\left(\frac{dT_C}{dx}\right)_{x=0} = -187.2\,K$ and $\left(\frac{dP_C}{dx}\right)_{x=0} = -2.05\,MPa$ at infinite dilution ($x \to 0$) calculated from Eqs. 3 and 4 were used to determine the value of the Krichevskii parameter for the $NH_3 + H_2O$ mixture. Our result for the Krichevskii parameter calculated with Eq. 5 is (48.16 ± 3) MPa. This means that when exchanging a solvent (water) molecule by one solute (ammonia) molecule at constant volume and temperature, the local density of water molecules around the ammonia molecule decreases when compared with the ideal mixture or bulk density of pure water. Therefore, a dilute $NH_3 + H_2O$ mixture is a "repulsive" mixture according to the classification by Levelt Sengers [79] and Debenedetti and Mohamed [83].

As will be shown below, the values of the partial molar volume at infinite dilution are also positive, while the cluster size is negative. Table 3 provides a comparison of the value of the Krichevskii parameter derived in this work with values reported by other authors. As one can see from Table 3, the agreement between various sources is sufficient. In Fig. 15 are presented the experimental dew- and bubble-pressure data of $NH_3 + H_2O$ mixtures as a function of concentration at constant temperature near the

Table 3 Values of the Krichevskii parameter $\left(\frac{\partial P}{\partial x}\right)^{\infty}_{T_C V_C}$ for aqueous ammonia solution

[117]	[120]	[118]	[119]	[29]	This study	This study	This study
52.0	45.9	44	41	43.6[a]	44.4[b]	48.2[c]	51.4[d]

[a] CREOS [29]
[b] VLE Experiment [48]
[c] Krichevskii Eq. 5
[d] Krichevskii Eq. 6

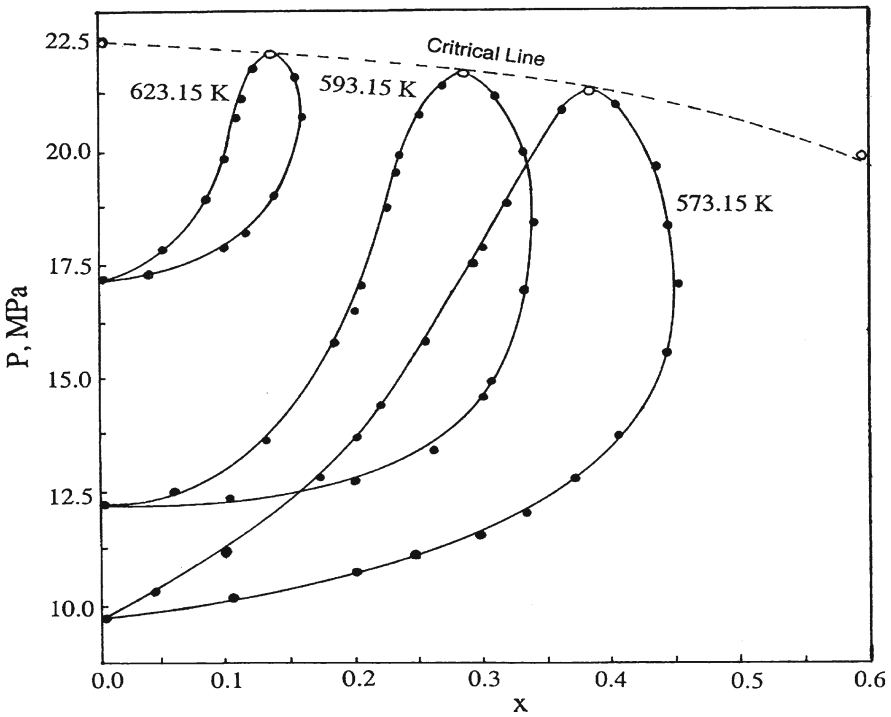

Fig. 15 Concentration dependence of the bubble-point and dew-point pressures (P_σ–x) for $NH_3 + H_2O$ mixture along the pure water's near-critical isotherm reported by Tsiklis et al. [48]; (—) *smoothed curves*, (- - -) critical curve

critical point of pure water reported by Tsiklis et al. [48]. Using these data, we calculated the initial slopes, $(\partial P_\sigma / \partial x)_{TV}$, of the dew- and bubble-point pressures at infinite dilution ($x \to 0$) for various fixed temperatures. The derived results for $(\partial P_\sigma / \partial x)_{TV}$ for various isotherms were extrapolated to the critical point of pure water to estimate the value of the Krichevskii parameter from direct P_σ–x measurements. The derived value of the Krichevskii parameter from the direct P_σ–x measurements is 44.4 MPa which agrees well with the present and other reported data.

4.2 Isomorphic Near-Critical Behavior of the Isochoric Heat Capacity of $NH_3 + H_2O$ Mixtures

The Krichevskii parameter or the shape of the critical lines also governs the thermodynamic behavior (isomorphism of the critical behavior of mixtures) of fluid mixtures near the critical point of one of the components. A comprehensive analysis of the consequences of the isomorphism principle to the critical behavior of mixtures has been presented by Anisimov et al. [105–108]. According to the isomorphism principle, the near-critical behavior of binary fluids (C_V and other thermodynamic properties) is controlled by two characteristic parameters, K_1 and K_2 [105–108], that are determined by the initial slopes ($x \to 0$) of the critical curves (T_C–x) and (P_C–x). The parameter K_1 controls strongly divergent properties such as the isothermal compressibility K_T and the isobaric heat capacity C_P. The parameter K_2 is responsible for the deformation of the weak divergence of C_V and defines the range of Fisher renormalization of the critical exponent α [109]. The parameter K_1 and the corresponding characteristic temperature difference τ_1 and the characteristic density difference $\Delta\rho_1$ are defined by [105–108] as

$$K_1 = \frac{x(1-x)}{\rho_C R T_C}\left[\frac{dP_C}{dx} - \left(\frac{dP_S}{dT}\right)^c_{CXC}\frac{dT_C}{dx}\right],\quad \tau_1 = \left[\frac{\Gamma_0^+ K_1^2}{x(1-x)}\right]^{1/\gamma} \quad \text{and} \quad \Delta\rho_1 = B_0\tau_1^\beta. \tag{7}$$

The isochoric heat-capacity behavior of a binary mixture will exhibit the same behavior as those of the pure components in the range of temperature $\tau \gg \tau_2$ [105–108], where

$$\tau_2 = \left[A_0^+ \frac{K_2^2}{x(1-x)}\right]^{1/\alpha},\quad K_2 = \frac{x(1-x)}{T_C(x)}\frac{dT_C}{dx},\quad \tau = \frac{T - T_C}{T},$$
$$\Delta\rho = \frac{\rho - \rho_C}{\rho_C},\quad \Delta\rho_2 = B_0\tau_2^\beta. \tag{8}$$

The value of the derivative $\frac{dT_C}{dx} = -191.72\,K$ at $x = 0.2607$ mole fraction of NH_3 is calculated from Eq. 3, the critical temperature for composition $x = 0.2607$ mole fraction of NH_3 is $T_C = 599.67\,K$, the critical amplitudes $A_0^+ = 31.2$, $B_0 = 1.98$, and $\Gamma_0^+ = 0.058$ of the power laws for isochoric heat capacity, coexistence curve, and isothermal compressibility for pure water, respectively, are from Ref. [110], and the universal critical exponents for $C_V, \alpha = 0.11$, and for the coexistence curve, $\beta = 0.324$, are from Ref. [66]. The values of characteristic parameters K_1, τ_1, $\Delta\rho_1$, K_2, τ_2, and $\Delta\rho_2$ calculated from Eqs. 7 and 8 for the 0.2607 NH_3 + 0.7393 H_2O mixture are as follows: $K_1 = 0.0978$; $K_2 = -0.0615$; $\tau_1 = 0.0089$; $\tau_2 = 0.0117$; $\Delta\rho_1 = 0.429$; and $\Delta\rho_2 = 0.469$. Along the critical isochore in the single-phase region, all the properties of a binary fluid mixture will exhibit the same behavior as those of a pure fluid in the range of temperatures $\tau \gg \tau_1$ and $\tau \gg \tau_2$. For the 0.2607 NH_3 + 0.7393 H_2O mixture, this occurs at $\tau \gg 0.0089$ (or 605.01 K) and $\tau \gg 0.0117$ (or 606.69 K), respectively.

For $\tau_2 < \tau < \tau_1$, properties that exhibit strong singularities in single-component fluids (associated with critical exponent γ) will reach a plateau; however, weakly singular properties (associated with critical exponent α) will continue to grow. At $\tau < \tau_2$ (0.0117), those properties that diverge weakly in single-component fluids will be saturated and all the critical exponents will be renormalized by a factor $1/(1-\alpha)$. In terms of density, along the critical isotherm, the behavior of all the properties will be single-component-like at densities $|\Delta\rho| \gg \pm\Delta\rho_1$ (0.429) and Fisher renormalization occurs at $|\Delta\rho| \ll \pm\Delta\rho_2$ (0.469). Figures 16 and 17 show the concentration dependence of the characteristic parameters, τ_1 and τ_2, and $\Delta\rho_1$ and $\Delta\rho_2$.

As one can see, the values of τ_2 at concentrations between 0.18 and 0.98 mole fraction show a maximum, while the characteristic temperature difference τ_1 is different from zero over the whole concentration range. Therefore, Fisher renormalization (mixture-like behavior) of the critical exponent for weakly singular properties such as C_V along the critical isochore can be experimentally observed at temperatures $\tau < \tau_2$ (for the $NH_3 + H_2O$ mixture with composition $x = 0.2603$ mole fraction NH_3 of $\tau < 0.0117$), while all the properties that exhibit strong singularities in single-component fluids exhibit pure-like behavior at temperatures $\tau > 0.0089$.

In terms of density, along the critical isotherm, C_{VX} exhibits mixture-like behavior at densities $|\Delta\rho| \ll 0.469$. Figure 18 shows a C_V–$\ln\tau$ plot of the isochoric heat capacity of the 0.2607 NH_3 + 0.7393 H_2O mixture and pure water along their critical densities. As this figure demonstrates, the mixture exhibits mixture-like behavior (renormalization), as the critical point is approached at temperatures of approximately $\tau < 0.0111$ which is fairly close to the value ($\tau = 0.0117$) predicted by critical properties data. In the concentration range from (0 to 0.18) mole fraction and from

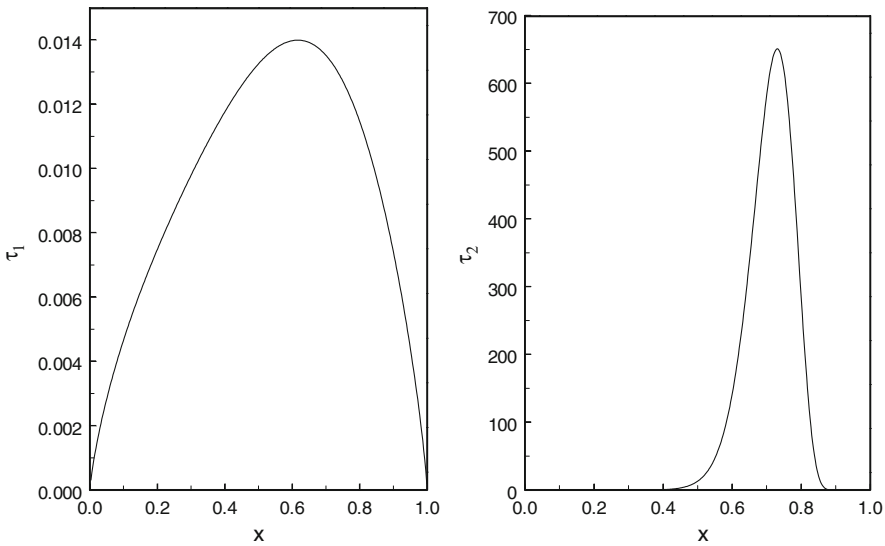

Fig. 16 Characteristic reduced temperatures τ_1 and τ_2 as a function of concentration calculated from the critical lines data, Eqs. 7 and 8

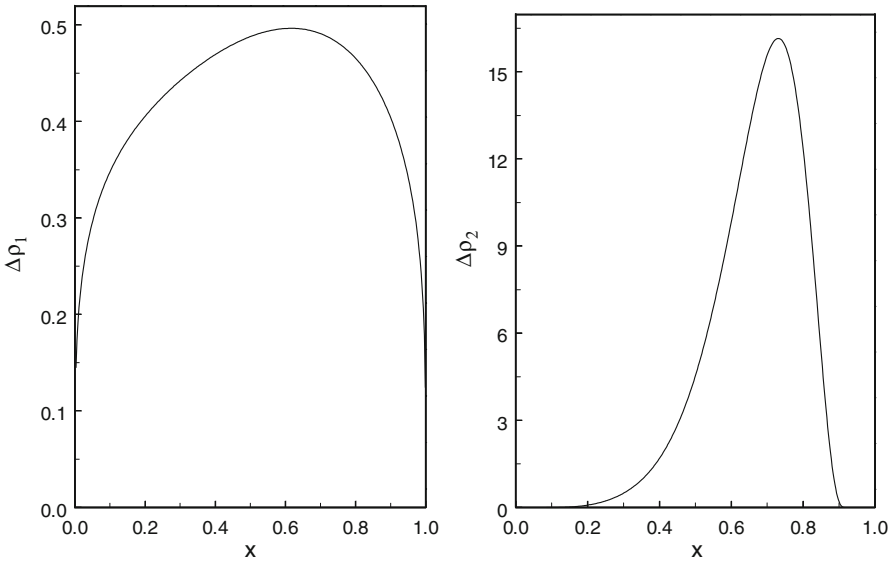

Fig. 17 Characteristic reduced densities $\Delta\rho_1$ and $\Delta\rho_2$ as a function of concentration calculated from the critical lines data, Eqs. 7 and 8

(0.98 to 1.0) mole fraction, the weakly singular properties (C_V) exhibit pure-like behavior ($C_V \propto \tau^{-\alpha}$), because in this concentration range, τ_2 is almost zero.

Unfortunately, there is no C_{VX} data for the mixture in these concentration ranges to check the pure-like behavior of the isochoric heat capacity along the critical isochore. However, it is physically obvious that as the concentration approaches the pure component limits ($x \to 0$ and $x \to 1$), the pure components in the mixture dominate the critical effects, displaying behavior which is typical for pure fluids. Therefore, in the concentration ranges of $x < 0.18$ and $x > 0.98$ mole fractions, the crossover from mixture-like to pure-like behavior of C_{VX} is observed along the critical isochore. This means that C_{VX}, which diverges weakly for pure H_2O ($x = 0$) and pure NH_3 ($x = 1$) with an exponent $\alpha = 0.110$, $C_V \propto \tau^{-\alpha}$, along the critical isochore, will be renormalized by the factor $1/(1-\alpha)$ ($-\alpha \Rightarrow \alpha/(1-\alpha)$), $C_{VX} \propto \tau^{\alpha/(1-\alpha)}$ for the 0.2607 NH_3 + 0.7393 H_2O mixture at concentrations between (0.18 and 0.98) mole fraction of ammonia at temperatures below τ_2 (see Fig. 16).

4.3 Thermodynamic and Structural Properties at Infinite Dilution of $NH_3 + H_2O$ Mixtures

The partial molar volume at infinite dilution $\bar{V}_2^{\infty}$ is a very fundamental mixture property (for example, to study solute–solvent interactions, where solvent–solvent interactions are vanishing) and can be expressed as a simple integral by using the direct correlation function [97]. For infinitely dilute mixtures ($x \to 0$), the partial molar volume of the solute $\bar{V}_2^{\infty}$ can be calculated using the concentration derivatives of pressure $\left(\frac{\partial P}{\partial x}\right)_{TV}^{\infty}$ (Krichevskii function) as [79,82,83,97,111,112]

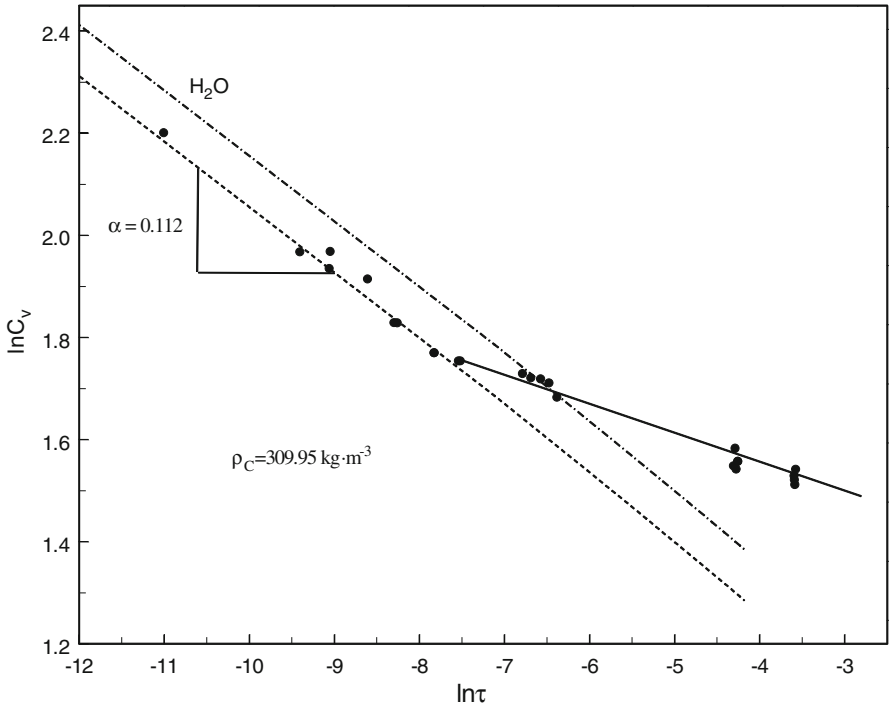

Fig. 18 Measured and calculated isochoric heat capacities of pure water and 0.2607 $NH_3 + 0.7393\,H_2O$ as a function of $\ln\tau$ along the critical isochore of mixture; The values for pure water (–·–·–·–) are calculated with the crossover equation of state by Kiselev and Friend [116], (—) and (– – – –) guide the eye; •—this study

$$\bar{V}_2^{\infty} = \rho_0^{-1}\left[K_T\left(\frac{\partial P}{\partial x}\right)_{TV}^{\infty} + 1\right], \tag{9}$$

where $K_T > 0$ is the compressibility of the pure solvent (water) and ρ_0 is the density of the pure solvent (water). As one can see from Eq. 9, adding a solute (ammonia) which will likely raise the pressure, $\left(\frac{\partial P}{\partial x}\right)_{TV}^{C} > 0$, will cause the partial molar volume $\bar{V}_2^{\infty}$ to approach $+\infty$. This anomaly is caused by the critical effects due to the divergence of the isothermal compressibility K_T of the pure solvent (water) and is common to all dilute near-critical mixtures. Near the critical point of pure water ($x \to 0$, infinite dilution), the Krichevskii function in Eq. 9, $\left(\frac{\partial P}{\partial x}\right)_{TV}^{\infty}$, approaches the Krichevskii parameter, and the isothermal compressibility strongly diverges at the critical point of the solvent (water) $K_T \propto (T - T_C)^{-\gamma} \to +\infty$; consequently, the partial molar volume $\bar{V}_2^{\infty}$ will also diverge strongly.

The sign of the $\bar{V}_2^{\infty}$ divergence is dependent on the sign of the Krichevskii parameter. For some solutes (relatively involatile), the partial molar volume tends to minus infinity $\bar{V}_2^{\infty} \to -\infty$ (for example, for most salt solutions). For these types of mixtures, the Krichevskii parameter, therefore, is negative. The calculated values with Eq. 9 of

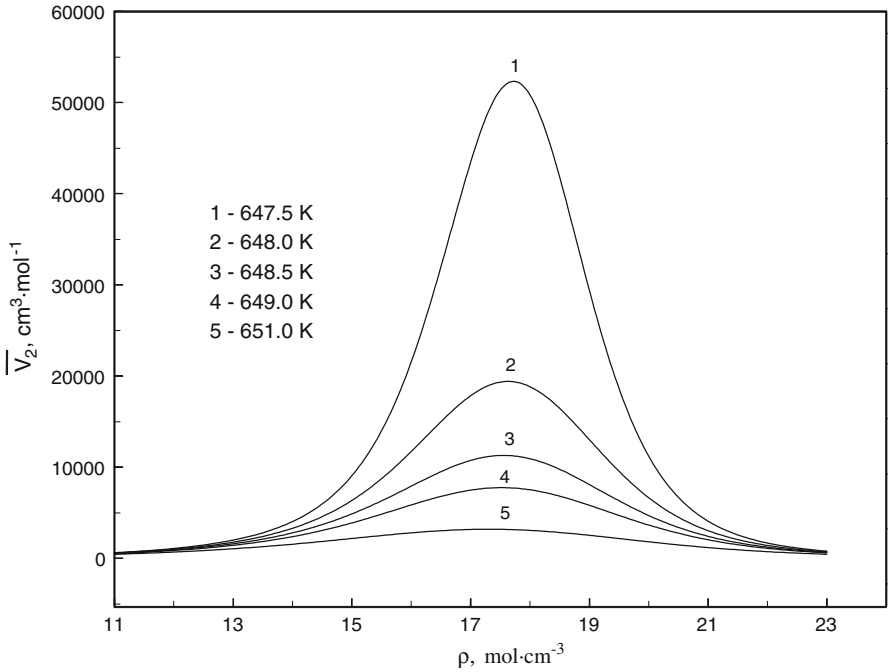

Fig. 19 Partial molar volumes $\bar{V}_2^{\infty}$ of NH_3 in infinite dilution $NH_3 + H_2O$ mixture as a function of pure water density ρ at fixed pure water near-critical and supercritical temperatures calculated from Eq. 9 using crossover model [29]

the partial molar volumes $\bar{V}_2^{\infty}$ at infinite dilution near the critical point of pure water as a function of density along the near- and supercritical isotherms are given in Fig. 19. Figure 20 shows comparisons of calculated and measured values of the partial molar volumes of NH_3 at infinite aqueous dilution along the selected near-critical isobar of 28 MPa. As this figure shows, the agreement between measured values [113] and those calculated with Eq. 9 is sufficient. Figure 20 also gives the values of $\bar{V}_2^{\infty}$ calculated with the model developed by O'Connell et al. [89].

The values of the Krichevskii function, $\left(\frac{\partial P}{\partial x}\right)_{TV}^{\infty}$, also associated with the behavior of the microstructure of the dilute mixture, represent a measure of the finite microscopic rearrangement of the solvent structure around the infinitely dilute solute relative to the solvent structure ideal solution. The Krichevskii function defines the structural properties of infinite dilute mixtures, namely, the excess number of solvent (water) molecules N_{exc}^{∞} (structural parameter) around the infinitely dilute solute (ammonia) relative to that number around any other solvent (water) molecule as [114,115]

$$N_{\text{exc}}^{\infty} = -K_T \left(\frac{\partial P}{\partial x}\right)_{TV}^{\infty}, \tag{10}$$

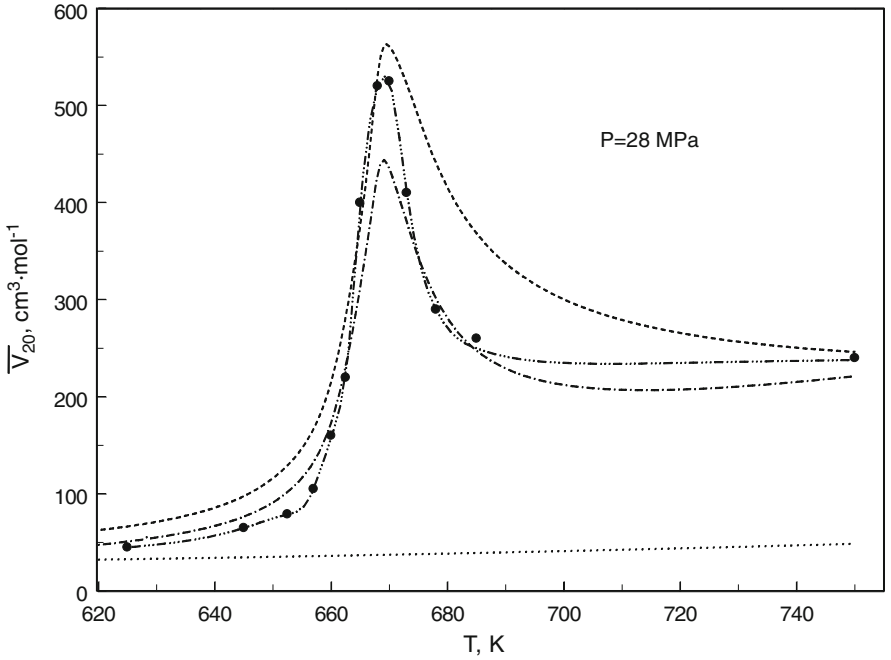

Fig. 20 Partial molar volumes of NH_3 in infinite dilution $NH_3 + H_2O$ mixture along the near-critical isobar as a function of temperature calculated with Eq. 9 using the crossover equation of state [29]; (–·–·–·–) this study from Eq. 9, (– – ––) O'Connell et al. [89], (· · · · ·) Gillespie et al. [51], (–·· ·●–·· ·●–·· ·) Hnedkovsky et al. [113]

where

$$N_{\mathrm{exc}}^{\infty} = 4\pi\rho \int_0^{R_{\mathrm{shell}}} [g_{12}(r) - g_{11}(r)] r^2 \mathrm{d}r, \tag{11}$$

is the definition of the excess number of solvent (water) molecules surrounding the ammonia molecule at infinite dilution. As one can see from Eq. 11, $N_{\mathrm{exc}}^{\infty} = N_{12} - N_{11}$, where $N_{12} = 4\pi\rho \int_0^{R_{\mathrm{shell}}} g_{12}(r) r^2 \mathrm{d}r$ and $N_{11} = 4\pi\rho \int_0^{R_{\mathrm{shell}}} g_{11}(r) r^2 \mathrm{d}r$ are the coordination numbers for the first solvation shell (molecule clusters). Figure 21 shows the density dependence of the excess number of solvent (water) molecules, $N_{\mathrm{exc}}^{\infty}$, around the infinitely dilute solute (ammonia) along the various supercritical isotherms calculated from Eq. 10 using the isothermal compressibility of pure water and the values of the Krichevskii function. As one can see from Fig. 21, the excess number of solvent (water) molecules $N_{\mathrm{exc}}^{\infty}$ around the ammonia molecule in the infinite dilution limit is negative (the Krichevskii parameter is positive). This means that when exchanging a solvent (water) molecule by one solute (ammonia) molecule at constant volume and temperature, the local density of water molecules around the ammonia molecule decreases when compared with the ideal mixture or bulk density of pure water. Thus, ammonia + water is a "repulsive" mixture, $\left(\frac{\partial P}{\partial x}\right)_{TV}^{\infty} > 0$ [79,83].

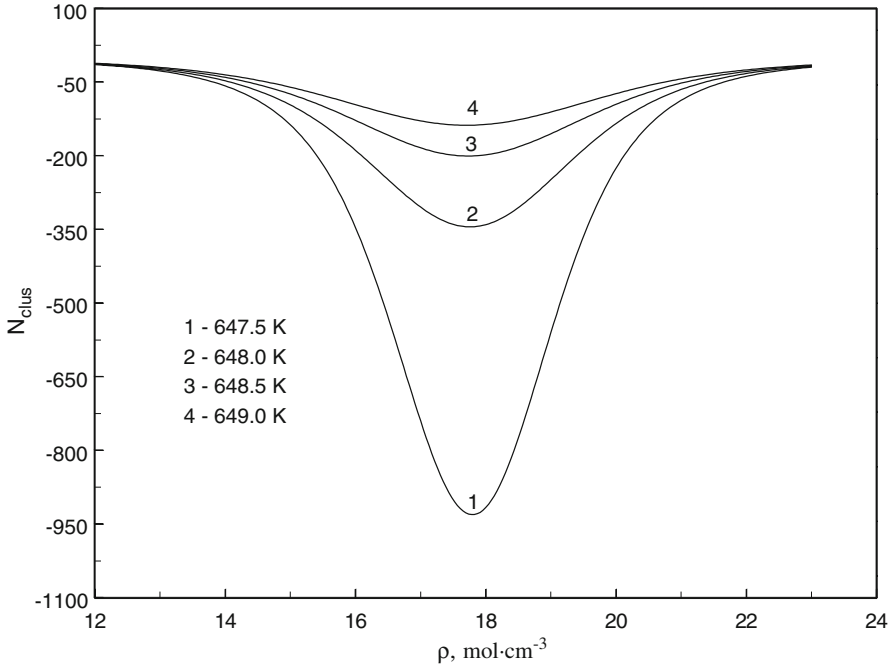

Fig. 21 Density dependence of the excess number of solvent (water) molecules, $N_{\mathrm{exc}}^{\infty}$, around the infinitely dilute solute (ammonia) along the various supercritical isotherms calculated from Eq. 10

5 Conclusions

Isochoric heat capacities ($C_V VT$), phase boundary (T_S, ρ_S) and critical (T_C, ρ_C) parameters for a 0.2607 NH_3 + 0.7393 H_2O mixture have been measured using a high-temperature, high-pressure, nearly constant-volume adiabatic calorimeter and quasi-static thermogram techniques. Measurements were made along liquid and vapor isochores between 120.03 kg · m^{-3} and 671.23 kg · m^{-3}. The range of temperature was (478 to 634) K. The derived values of the critical parameter for the mixture are T_C = (599.67 ± 0.2) K and ρ_C = (310.95 ± 5) kg · m^{-3}. The value of the Krichevskii parameter (48.16 ± 3) MPa was calculated using the critical line data. The value of the Krichevskii parameter is positive and the partial molar volumes at infinite dilution for this mixture are positively diverging, while the values of the cluster size are negatively diverging. The values of the characteristic parameters ($K_1 = 0.0978$, $K_2 = -0.0615$, $\tau_1 = 0.0089$, $\tau_2 = 0.0117$, $\Delta\rho_1 = 0.429$, and $\Delta\rho_2 = 0.469$) for the 0.2607 NH_3 + 0.7393 H_2O mixture are calculated using the present and reported values of the critical properties data.

The isochoric heat capacity of the $NH_3 + H_2O$ mixture exhibits pure-like behavior ($C_V \propto \tau^{-\alpha}$) along the critical isochore at concentrations $x > 0.98$ and $x < 0.18$ mole fraction. All the strongly divergent properties such as the isothermal compressibility K_T and the isobaric heat capacity C_P exhibit pure-like behavior along the critical isochore at temperatures $\tau > 0.0089$. In the concentration range between

(0.18 and 0.98) mole fraction along the critical isochore at temperatures $\tau < \tau_2$, C_{VX} exhibits mixture-like behavior (Fisher renormalization of the critical behavior, $\alpha \to 1/(1-\alpha)$, is taking place). For this mixture ($x = 0.2607$ mole fraction of ammonia), the value of τ_2 is 0.0117. In terms of density, along the critical isotherm C_{VX}, this $0.2607\,NH_3 + 0.7393\,H_2O$ mixture exhibits mixture-like behavior ($C_{VX} \propto \tau^{\alpha/(1-\alpha)}$) at densities $|\Delta\rho| \ll 0.469$.

Acknowledgments I. M. Abdulagatov thanks the Thermophysical Properties Division at the National Institute of Standards and Technology for the opportunity to work as a Guest Researcher at NIST during the course of this research. This study was also supported by the Grant from the Russian Foundation of Basic Research RFBR 08-08-12258. The authors also thank Dr. J. W. Magee for his help in promoting this study and for useful discussions.

References

1. M. Jonsson, *Ph. D. Thesis* (RIT, Stockholm, Sweden, 2003)
2. E. Thorin, *Ammonia–Water Mixtures as Working Fluid in Power Cycles* (RIT, Stockholm, 1998)
3. E. Thorin, *Ph. D. Thesis* (RIT, Stockholm, 2000)
4. E. Thorin, C. Dejfors, G. Svedberg, Int. J. Thermophys. **19**, 501 (1998)
5. Y.M. Park, R.E. Sonntag, Int. J. Energy Res. **14**, 153 (1990)
6. A.I. Kalina, H.M. Leibowitz, Geothermal Resour. Council, Trans. **13**, 605 (1989)
7. K. Gawlik, V. Hassani, *Geothermal Resources Council, Annual Meeting* (San Diego, CA, 20–23 September 1998)
8. E.K. Olsson, E.B. Thorin, A.S. Dejfors, G. Svedberg, in *Proceedings Florence World Energy Research Symposium* (Florence, Italy, 6–8 July 1994), pp. 39–49
9. V. Hassani, J. Dickens, Y. Parent, *Ammonia/Water Condensation Test: Plate-Fin Heat Exchanger (Absorber/Cooler)* (NREL, Golden, CO, September 2001)
10. M. Jonsson, E. Thorin, G. Svedberg, in *Proceedings Florence World Energy Research Symposium* (Florence, Italy, 6–8 July 1994), pp. 1–11
11. Y. Amano, T. Hashizume, Y. Tanzawa, T. Suzuki, M. Akiba, A. Usui, in *Proceedings 2000 International Joint Power Generation Conference* (Miami Beach, FL, 23–26 July 2000), pp. 1–6
12. Y. Amono, in *Proceedings 1999 International Joint Power Generation Conference—ICOPE ASME/JSME PWR*, vol. 34 (1999), p. 67
13. A.S. Dejfors, E. Thorin, G. Svedberg, Energy Convers. Mgmt. **39**, 1675 (1998)
14. G. Wall, Ch.-Ch. Chuang, M. Ishida, in *Analysis and Design of Energy Systems: Analysis of Industrial Processes*, ed. by R.A. Bajura, M.R. von Spakovsky, E.S. Geskin, vol. 10-3 (AES, ASME, 2000), pp. 73–77
15. R. Tillner-Roth, D.G. Friend, J. Phys. Chem. Ref. Data **27**, 45 (1998)
16. N.G. Polikhronidi, I.M. Abdulagatov, J.W. Magee, R.G. Batyrova, J. Chem. Eng. Data **46**, 1064 (2001)
17. N.G. Polikhronidi, I.M. Abdulagatov, J.W. Magee, G.V. Stepanov, Int. J. Thermophys. **22**, 189 (2001)
18. N.G. Polikhronidi, I.M. Abdulagatov, J.W. Magee, G.V. Stepanov, Int. J. Thermophys. **23**, 745 (2002)
19. N.G. Polikhronidi, I.M. Abdulagatov, J.W. Magee, G.V. Stepanov, Int. J. Thermophys. **24**, 405 (2003)
20. N.G. Polikhronidi, I.M. Abdulagatov, R.G. Batyrova, Fluid Phase Equilib. **201**, 269 (2002)
21. N.G. Polikhronidi, I.M. Abdulagatov, G.V. Stepanov, R.G. Batyrova, Fluid Phase Equilib. **252**, 33 (2007)
22. N.G. Polikhronidi, R.G. Batyrova, I.M. Abdulagatov, J.W. Magee, G.V. Stepanov, J. Supercrit. Fluids **33**, 209 (2004)
23. N.G. Polikhronidi, R.G. Batyrova, I.M. Abdulagatov, Fluid Phase Equilib. **175**, 153 (2000)
24. N.G. Polikhronidi, R.G. Batyrova, I.M. Abdulagatov, Int. J. Thermophys. **21**, 1073 (2000)
25. N.G. Polikhronidi, I.M. Abdulagatov, J.W. Magee, G.V. Stepanov, Int. J. Thermophys. **27**, 729 (2006)
26. N.G. Polikhronidi, G.V. Stepanov, I. M. Abdulagatov, R.G. Batyrova, Thermochim. Acta **454**, 99 (2007)
27. J.W. Magee, N. Kagawa, J. Chem. Eng. Data **43**, 1082 (1998)
28. R. Tillner-Roth, D.G. Friend, J. Phys. Chem. Ref. Data **27**, 63 (1998)

29. S.B. Kiselev, J.C. Rainwater, Fluid Phase Equilib. **141**, 129 (1997)
30. J.C. Rainwater, R. Tillner–Roth, in *Proceeding 13th IAPWS Conference, Steam, Water, and Hydrothermal Systems: Physics and Chemistry Meeting the Needs of Industry*, ed. by P.R. Tremaine, P.G. Hill, D.E. Irish, P.V. Balakrishnan (NRC Research Press, Ottawa, 2000), pp. 110–117
31. R. Peters, J.U. Keller, DKV-Tagungsber **2**, 183 (1993)
32. T.M. Smolen, D.B. Manley, B.E. Poling, J. Chem. Eng. Data **36**, 202 (1991)
33. H. Huang, Fluid Phase Equilib. **58**, 93 (1990)
34. Z. Duan, N. Moller, J.H. Weare, J. Solut. Chem. **25**, 43 (1996)
35. V. Abovsky, Fluid Phase Equilib. **116**, 170 (1996)
36. M. Moshfeghian, A. Shariat, R.N. Maddox, Fluid Phase Equilib. **80**, 33 (1992)
37. D.G. Friend, A.L. Olson, A. Nowarski, Int. J. Thermophys. **19**, 1133 (1998)
38. Y. Ikegami, T. Nishida, M. Uto, H. Uehara, in *Proceedings 13th Japan Symposium Thermophysical Properties* (Tokyo, 1992), p. 213
39. J. Paték, J. Klomfar, Int. J. Refrig. **18**, 228 (1995)
40. R.M. Enick, G.P. Donahey, M. Holsinger, Ind. Eng. Chem. Res. **37**, 1644 (1998)
41. K. Thomsen, P. Rasmussen, in *Proceedings 13th IAPWS Conference, Steam, Water, and Hydrothermal Systems: Physics and Chemistry Meeting the Needs of Industry*, ed. by P.R. Tremaine, P.G. Hill, D.E. Irish, P.V. Balakrishnan (NRC Research Press, Ottawa, 2000), pp. 118–125
42. J. Suzuki, M. Uematsu, Heat Transfer-Asian Res. **31**, 320 (2002)
43. M. Barhoumi, A. Snoussi, N. Ben Ezzine, K. Mejbri, A. Bellagi, Int. J. Refrig. **27**, 271 (2004)
44. F. Xu, D.Y. Goswami, Energy **24**, 525 (1999)
45. Kh. Mejbri, A. Bellagi, Int. J. Refrig. **29**, 211 (2006)
46. S.S. Rizvi, A. Heidemann, J. Chem. Eng. Data **32**, 183 (1987)
47. C.L. Sassen, R.A.C. van Kwartel, H.J. van der Kool, J. de Swaan Arons, J. Chem. Eng. Data **35**, 140 (1990)
48. D.S. Tsiklis, L.R. Linshitts, N.P. Gorinova, Russian J. Phys. Chem. **39**, 2978 (1965)
49. S. Postma, Rec. Trav. Chim. **39**, 515 (1920)
50. A. Sakabe, D. Arai, H. Miyamoto, M. Uematsu, J. Chem. Thermodyn. **40**, 1527 (2008)
51. P.C. Gillespie, W.V. Wilding, G.M. Wilson, AIChE Symp. Ser. **256**, 83 (1987–1989)
52. Kh.I. Amirkhanov, G.V. Stepanov, B.G. Alibekov, *Isochoric Heat Capacity of Water and Steam* (Amerind Publishing Co., New Delhi, 1974)
53. Kh.I. Amirkhanov, G. V. Stepanov, I.M. Abdulagatov, O.A. Buyi, *Isochoric Heat Capacity of Propyl and Isopropyl Alcohols* (Dagestan Scientific Center of the Russian Academy of Sciences Publication, Makhachkala, 1989)
54. I.M. Abdulagatov, N.G. Polikhronidi, T.J. Bruno, R.G. Batyrova, G.V. Stepanov, Fluid Phase Equilib. **263**, 71 (2008)
55. I.K. Kamilov, G.V. Stepanov, I.M. Abdulagatov, A.R. Rasulov, E.M. Milikhina, J. Chem. Eng. Data **46**, 1556 (2001)
56. N.G. Polikhronidi, I.M. Abdulagatov, J.W. Magee, G.V. Stepanov. Int. J. Thermophys. **22**, 189 (2001)
57. N.G. Polikhronidi, I.M. Abdulagatov, J.W. Magee, G.V. Stepanov, Int. J. Thermophys. **23**, 745 (2002)
58. N.G. Polikhronidi, I.M. Abdulagatov, J.W. Magee, G.V. Stepanov. Int. J. Thermophys. **24**, 405 (2003)
59. N.G. Polikhronidi, I.M. Abdulagatov, R.G. Batyrova. Fluid Phase Equilib. **201**, 269 (2002)
60. N.G. Polikhronidi, R.G. Batyrova, I.M. Abdulagatov, Int. J. Thermophys. **21**, 1073 (2000)
61. N.G. Polikhronidi, R.G. Batyrova, I.M. Abdulagatov, J.W. Magee, G.V. Stepanov, J. Supercrit. Fluids **33**, 209 (2004)
62. N.G. Polikhronidi, R.G. Batyrova, I.M. Abdulagatov. Fluid Phase Equilib. **175**, 153 (2000)
63. I.M. Abdulagatov, S.B. Kiselev, J.F. Ely, N.G. Polikhronidi, A.A. Abdurashidova. Int. J. Thermophys. **26**, 1327 (2005)
64. N.G. Polikhronidi, G.V. Stepanov, I.M. Abdulagatov, R.G. Batyrova, Thermochim. Acta **454**, 99 (2007)
65. V.M. Valyashko, I.M. Abdulagatov, J.M.H. Levelt- Sengers, J. Chem. Eng. Data **45**, 1139 (2000)
66. J.V. Sengers, J.M.H. Levelt Sengers, Ann. Rev. Phys. Chem. **37**, 189 (1986)
67. J. Rowlinson, F.L. Swinton, *Liquids and Liquid Mixtures*, 3rd edn. (Butterworths, London, 1982)
68. Ya.R. Chashkin, V.A. Smirnov, A.V. Voronel, *Thermophysical Properties of Substances and Materials*, vol. 2 (GSSSD, Moscow, 1970), p. 139
69. A.V. Voronel, in *Phase Transitions and Critical Phenomena*, ed. by C. Domb, M.S. Green, vol. 5 (Academic Press, London, 1974), p. 343

70. W. Wagner, A. Pruß, J. Phys. Chem. Ref. Data **31**, 387 (2002)
71. J.M.H. Levelt Sengers, J. Straub, K. Watanabe, P.G. Hill, J. Phys. Chem. Ref. Data **14**, 193 (1985). The Revised Values, on ITS-90, can be found in Physical Chemistry of Aqueous Systems, ed. by H.J. White Jr., J.V. Sengers, D.B. Neumann, J.C. Bellows (Begell House, New York, 1995), pp. A101–A102 (Appendix)
72. A.S. Teja, M.J. Anselme, AIChE Symp. Ser. **86**, 115 (1990)
73. R.D. Chirico, W.V. Steele, Ind. Eng. Chem. Res. **33**, 157 (1994)
74. J.G. Roof, J. Chem. Eng. Data **15**, 301 (1970)
75. M.T. Ratzsch, G. Strauch, Z. Phys. Chem. (Leipzig) **249**, 243 (1972)
76. R. Tillner-Roth, F. Harms-Watzenberg, H.D. Baehr, DKV-Tagungsbericht **20**, 167 (1993)
77. H.D. Baehr, R. Tillner-Roth, *Thermodynamic Properties of Environmentally Acceptable Refrigerants; Equations of State and Tables for Ammonia, R22, R134a, R152a, and R123* (Springer, Berlin, 1994)
78. J.M.H. Levelt Sengers, in *Supercritical Fluids: Fundamentals for Applications*, ed. by E.Kiran, J.M.H. Levelt Sengers (Kluwer, Dordrecht, 1994), pp. 3–38
79. J.M.H. Levelt Sengers, J. Supercrit. Fluids **4**, 215 (1991)
80. J.M.H. Levelt Sengers, in *Supercritical Fluid Technology*, ed. by J.F. Ely, T.J. Bruno (CRC Press, Boca Raton, FL, 1991), pp. 1–56
81. J.M.H. Levelt Sengers, G. Morrison, G. Nielson, R.F. Chang, C.M. Everhart, Int. J. Thermophys. **7**, 231 (1986)
82. A.A. Chialvo, P.T. Cummings, AIChE J. **40**, 1558 (1994)
83. P.G. Debenedetti, R.S. Mohamed, J. Chem. Phys. **90**, 4528 (1989)
84. M.L. Japas, J.L. Alvarez, K. Gutkowski, R. Fernández-Prini, J. Chem. Thermodyn. **30**, 1603 (1998)
85. J.L. Alvarez, R. Fernandez-Prini, M.L. Japas, Ind. Eng. Chem. Res. **39**, 3625 (2000)
86. R.F. Chang, G. Morrison, J.M.H. Levelt Sengers, J. Phys. Chem. **88**, 3389 (1984)
87. M.A. Anisimov, J.V. Sengers, J.M.H. Levelt Sengers, in *The Physical and Chemical Properties of Aqueous Systems at Elevated Temperatures and Pressures: Water, Steam and Hydrothermal Solutions*, ed. by D.A. Palmer, R. Fernadez-Prini, A.H. Harvey (Elsevier, Amsterdam, 2004), pp. 29–71
88. R.F. Chang, J.M.H. Levelt Sengers, J. Phys. Chem. **90**, 5921 (1986)
89. J.P. O'Connell, A.V. Sharygin, R.H. Wood, Ind. Eng. Chem. Res. **35**, 2808 (1996)
90. E.H. Chimowitz, G. Afrane, Fluid Phase Equilib. **120**, 167 (1996)
91. J.C. Wheeler, Ber. Bunsenges. Phys. Chem. **76**, 308 (1972)
92. N.E. Khazanova, E.E. Sominskaya, Russ. J. Phys. Chem. **45**, 1485 (1971)
93. U. van Wasen, I. Swaid, G.M. Schneider, Angew. Chem. Int. Ed. Eng. **19**, 575 (1980)
94. R. Fernández-Prini, M.L. Japas, Chem. Soc. Rev. **23**, 155 (1994)
95. A.H. Harvey, J. Phys. Chem. **94**, 8403 (1990)
96. M.L. Japas, R. Fernandez-Pirini, J. Horita, D.J. Wesolowski, J. Phys. Chem. **99**, 5171 (1995)
97. A.A. Chialvo, P.T. Cummings, Mol. Phys. **84**, 41 (1995)
98. A.A. Chialvo, in *Fluctuation Theory of Mixtures*, ed. by E. Matteoli, G.A. Mansoori (Taylor and Francis, New York, 1990), p. 131
99. A.A. Chialvo, J. Phys. Chem. **95**, 6683 (1991)
100. J.P. O'Connell, Y. Hu, K.A. Marshall, Fluid Phase Equilib. **158**, 583 (1999)
101. H.D. Cochran, L.L. Lee, D.M. Pfund, in *Fluctuation Theory of Mixtures*, ed. by E. Matteoli, G.A. Manssori (Taylor and Francis, New York, 1990), p. 69
102. E.Z. Hamod, G.A. Manssori, in *Fluctuation Theory of Mixtures*, ed. by E. Matteoli, G.A. Mansoori (Taylor and Francis, New York, 1990), p. 95
103. I.R. Krichevskii, Russ. J. Phys. Chem. **41**, 1332 (1967)
104. J.M.H. Levelt-Sengers, in *Physical Chemistry of Aqueous Systems. Proceeding 12th International Conference Properties of Water and Steam*, ed. by H.J. White, J.V. Sengers, D.B. Neumann, J.C. Bellows (Begell House, New York, 1995), pp. A143–149
105. M.A. Anisimov, *Critical Phenomena in Liquids and Liquid Crystals* (Gordon and Breach, Philadelphia, 1991)
106. M.A. Anisimov, E.E. Gorodezkii, V.D. Kulikov, J.V. Sengers, Phys. Rev. E. **51**, 1199 (1995)
107. M.A. Anisimov, E.E. Gorodezkii, V.D. Kulikov, A.A. Povopdyrev, J.V. Sengers, Phys. A **220**, 277 (1995)
108. M.A. Anisimov, J.V. Sengers, in *Equations of State for Fluids and Fluids Mixtures*, ed. by J.V. Sengers, R.F. Kayser, C.J. Peters, H.J. White (Elsevier, Amsterdam, 2000), p. 381
109. M.E. Fisher, Phys. Rev. B **176**, 257 (1968)

110. M.A. Anisimov, A.A. Povodyrev, J.P. Roseli, J.V. Sengers, S.B. Kiselev, D.F. Friend, in *Proceedings 13th International Conference Properties of Water and Steam,* ed. by P.R. Tremaine, P.G. Hill, D.E. Irish, P.V. Balakrishnan (NRC Research Press, Ottawa, 2000), pp. 339–346
111. P.T. Cummings, A.A. Chialvo, Chem. Eng. Sci. **49**, 2735 (1994)
112. P.G. Debenedetti, S.K. Kumar, AIChE J. **34**, 645 (1984)
113. L. Hnedkovsky, R.H. Wood, V. Majer, J. Chem. Thermodyn. **28**, 575 (1995)
114. S.W. Brelvi, J.P. O'Connell, AIChE J. **18**, 1239 (1972)
115. D.B. Mcguigan, P.A. Monson, Fluid Phase Equilib. **57**, 227 (1990)
116. S.B. Kiselev, D.G. Friend, Fluid Phase Equilib. **155**, 33 (1999)
117. A.V. Plyasunov, E.L. Shock, J. Supercrit. Fluids **20**, 91 (2001)
118. A.V. Plyasunov, E.L. Shock, Geochim. Cosmochim. Acta **67**, 4981 (2003)
119. J. Alvarez, H.R. Corti, R. Fernandez-Prini, M.L. Japas, Geochim. Cosmochim. Acta **58**, 2789 (1994)
120. I.M. Abdulagatov, M.N. Dadashev, M.B. Saidalhmedova, Russ. Chem. Chem. Product. **1-2**, 30 (1998)